1 **Distinct Vegfa isoforms control endothelial cell proliferation through PI3 kinase signalling**

2 **mediated regulation of cdkn1a/p21**

3

4 Martin Lange[1,2,4], Elvin Leonard[1,2], Nils Ohnesorge[1,2], Dennis Hoffmann[1,2,6], Susana F. Rocha[5],

5 Rui Benedito[5] and Arndt F. Siekmann[1,2,3],*

6

7 **Affiliations**

8 [1]Max Planck Institute for Molecular Biomedicine, Roentgenstrasse 20, D-48149 Muenster, Germany

9 [2]Cells-in-Motion Cluster of Excellence (EXC 1003 – CiM), University of Muenster, Muenster, Germany

10 [3]Department of Cell and Developmental Biology and Cardiovascular Institute, Perelman School of Medicine at the

11 University of Pennsylvania, Philadelphia, PA, USA

12 [4]current address: Cardiovascular Research Center, Yale University School of Medicine, CT, USA

13 [5] Centro Nacional de Investigaciones Cardiovasculares (CNIC), Madrid, E28029, Spain

14 [6]current address: Institute for Cell Biology, ZMBE, Von-Esmarch-Street 56, 48149 Muenster, Germany

15 *Author for correspondence

16

17 Corresponding author:

18 Dr. Arndt F. Siekmann

19 email: arndt.siekmann@pennmedicine.upenn.edu

20 phone: +1 215 898 7805

21

22 **Key words: zebrafish, angiogenesis, Vegf signalling, PI3 kinase signalling, cdkn1a/p21,**

23 **endothelial cell proliferation**

24

1   **SUMMARY**

2   The formation of appropriately patterned blood vessel networks requires endothelial cell

3   migration and proliferation. Signaling through the Vascular Endothelial Growth Factor A

4   (VEGFA) pathway is instrumental in coordinating these processes. mRNA splicing generates

5   short (diffusible) and long (extracellular matrix bound) Vegfa isoforms. The differences between

6   these isoforms in controlling cellular functions are not understood. In zebrafish, *vegfaa* generates

7   short and long isoforms, while *vegfab* only generates long isoforms. We found that mutations in

8   *vegfaa* affected endothelial cell migration and proliferation. Surprisingly, mutations in *vegfab*

9   specifically reduced endothelial cell proliferation. Analysis of downstream signaling revealed no

10 change in MAPK (ERK) activation, while inhibiting PI3 kinase signaling phenocopied *vegfab*

11 mutants. The cell cycle inhibitor *cdkn1a/p21* was upregulated in *vegfab* deficient embryos.

12 Accordingly, reducing *cdkn1a/p21* restored endothelial cell proliferation. Together, these results

13 suggest that extracellular matrix bound Vegfa acts through PI3K signaling to specifically control

14 endothelial cell proliferation during angiogenesis independently of MAPK (ERK) regulation.

1 **INTRODUCTION**

2 The vascular system supplies our bodies with oxygen and nutrients to ensure efficient tissue

3 homeostasis. In order to fulfil these functions, appropriate numbers of blood vessels need to be

4 generated in the embryo or maintained during adulthood (Adams and Alitalo, 2007; Dejana et

5 al., 2017; Potente et al., 2011). The overproduction of blood vessels can lead to age-related

6 macular degeneration (Mitchell et al., 2018), diabetic retinopathy (Wong et al., 2016) or cancer

7 growth (Viallard and Larrivee, 2017). Formation of an insufficient number of blood vessels on

8 the other hand can cause hypoxia, resulting in tissue damage as seen in atherosclerotic

9 complication (Gimbrone and Garcia-Cardena, 2016).

10 Members of the vascular endothelial growth factor (VEGF) family are established

11 regulators of vascular development (Alvarez-Aznar et al., 2017; Koch and Claesson-Welsh,

12 2012; Simons et al., 2016). For instance, the formation of new blood vessels from pre-exiting

13 ones, termed angiogenesis, heavily relies on VEGFA and its receptor VEGFR2 (Kdr or Flk1).

14 Accordingly, heterozygous *Vegfa* mutant mice die in utero with vascular defects (Carmeliet et

15 al., 1996; Ferrara et al., 1996). Subsequent studies showed that VEGFA controls differentiation,

16 sprouting, migration, proliferation and survival of endothelial cells (ECs). Despite the

17 identification of several downstream players, such as Phosphoinositide 3-kinase (PI3K)

18 (Graupera and Potente, 2013) and Mitogen-activated protein kinase (MAPK/ERK) (Simons et

19 al., 2016), it is not known how VEGF signalling can differentially activate these pathways and

20 how this activation might lead to the observed broad array of cellular outcomes. For example, the

21 PI3K pathway controls EC survival in response to VEGFA in cultured cells (Gerber et al., 1998;

22 Nakatsu et al., 2003), while *in vivo* studies in the developing mouse retina (Graupera et al., 2008)

23 and in zebrafish embryos (Nicoli et al., 2012) suggested that PI3K signalling predominantly

3

1   regulates EC migration. More recent studies, however, also suggested a function of PI3K

2   signalling in EC proliferation during retinal development (Angulo-Urarte et al., 2018; Ola et al.,

3   2016) and in vascular malformations (Castel et al., 2016; Castillo et al., 2019; Castillo et al.,

4   2016). Further work in mouse and in cell culture has shown that ERK signalling downstream of

5   VEGFA stimulates EC proliferation (Koch and Claesson-Welsh, 2012), vessel integrity (Ricard

6   et al., 2019) and artery formation (Simons and Eichmann, 2015). Another study in zebrafish

7   embryos, however, implicated ERK signalling mainly in regulating EC migration, being

8   dispensable for early artery differentiation (Shin et al., 2016). Therefore, we still lack an

9   understanding of the sequence of downstream VEGF signalling events that occur during blood

10 vessel formation. We also do not understand how these might be triggered in different EC

11 populations through differential ERK and PI3K signalling.

12   One key aspect of VEGFA biology is the existence of differentially spliced isoforms

13 (Bowler and Oltean, 2019). Longer isoforms bind heparin and are associated with the

14 extracellular matrix (ECM), while the short, 121 amino acid (aa) isoform is diffusible (Vempati

15 et al., 2014). Studies in mice have shown that these isoforms differentially affect blood vessel

16 formation. Genetically engineered mice, which only express the VEGFA165 isoform are viable

17 (Stalmans et al., 2002), while mice expressing only VEGFA121 show angiogenesis defects

18 (Carmeliet et al., 1999; Ruhrberg et al., 2002; Stalmans et al., 2002). Thus, the ability to

19 associate with the extracellular matrix might change VEGFA downstream signalling and/or

20 gradient formation, as shown in cultured cells (Chen et al., 2010).

21   Zebrafish contain two *vegfa* paralogs, *vegfaa* and *vegfab*, likely being generated during a

22 genome duplication event (Taylor et al., 2003; Taylor et al., 2001). Both genes are expressed

23 during early embryogenesis and encode differentially spliced gene products, with *vegfaa*

1   encoding 121- and 165 aa isoforms (Gong et al., 2004; Liang et al., 1998), and *vegfab* encoding

2   171 and 210 aa isoforms (Bahary et al., 2007). Therefore, while *vegfaa* generates both diffusible

3   and ECM bound isoforms, *vegfab* only generates ECM bound isoforms. Here, we have generated

4   zebrafish mutants for *vegfaa* and *vegfab*. We find that, in agreement with studies in mice, *vegfaa*

5   is haploinsufficient. By contrast, *vegfab* mutants showed only mild vascular defects and survived

6   to adulthood. Surprisingly, however, EC proliferation was specifically affected in *vegfab*

7   mutants. Using inhibitor treatments and time-lapse analysis of vascular development, we show

8   that this phenotype was caused by impaired PI3K signalling without altering ERK activation.

9   Further analysis of downstream targets identified the cell cycle regulator Cdkn1a/p21 as a PI3K

10 target. Finally, we show that inhibition of PI3K signalling in the mouse retina similarly affected

11 EC proliferation. Together, our studies support a model, in which activation of PI3K signalling

12 downstream of ECM bound VEGFA is necessary to allow for optimal EC proliferation during

13 angiogenesis that is independent of signalling through ERK.

14

15 **RESULTS**

16 **Vegfaa and Vegfab mutants show distinct defects during brain blood vessel formation**

17 In order to investigate the role of each of the zebrafish *Vegfa* homologues during angiogenesis,

18 we generated zinc finger (for *vegfaa*) or TALEN (for *vegfab*) mutants, targeting the first exon of

19 either gene. We recovered two frameshift mutations, leading to severely truncated proteins of 18

20 (*vegfaa_{mu128}*) or 12 amino acids (*vegfab_{mu155}*), respectively (Figure 1A, B). To assess changes in

21 vascular morphology, we crossed both mutant lines into the *Tg(kdrl:EGFP)_{s843}* background,

22 expressing EGFP in ECs (Jin et al., 2005). We first focused our analysis on the developing

23 hindbrain vasculature (Figure 1C), which relies on VEGFR2 signaling (Bussmann et al., 2011;

1   Fujita et al., 2011; Ulrich et al., 2011). The arterial pole of the hindbrain vasculature forms via

2   two successive sprouting events emanating from the primordial hindbrain channels (PHBC),

3   two laterally located veins (Bussmann et al., 2011; Fujita et al., 2011; Ulrich et al., 2011). The

4   first sprouting event generates the medially located basilar artery (BA), while the second event

5   subsequently generates central arteries (CtAs), which connect the PHBCs with the BA (Figure

6   1D-F; Video S1). Both *vegfa* genes show distinct expression domains in the brain, as shown by

7   fluorescence in situ hybridization at 32 hpf. We detected expression of *vegfaa* dorsal to the

8   PHBC at positions of forming CtAs (Figure S1A, arrows, B). For *vegfab*, expression was

9   evident in the midline region, where the BA would form (Figure S1C, arrowheads, D) and

10   dorsally of the PHBCs (Figure S1C, arrows, D).

11   In line with these gene expression data, we observed specific vascular defects in each

12   mutant. Homozygous *vegfaa*$_{mu128}$ mutants showed a significant decrease in CtA numbers, while

13   these were unaffected in *vegfab*$_{mu155}$ mutants (Figure 1 G-L, quantified in Figure 1P; Videos S2

14   and S3). By contrast, the BA failed to form in these mutants, as previously reported (Rossi et al.,

15   2016). Its formation was unaffected in *vegfaa*$_{mu128}$ mutants (Figure 1G-L). To analyse whether

16   *vegfab* can contribute to CtA formation, we analysed *vegfaa*$_{mu128}$; *vegfab*$_{mu155}$ double mutants.

17   These showed a complete lack of BA and CtAs, while the PHBCs still formed (Figure 1M-O,

18   quantified in Figure 1P). These results suggest that during brain blood vessel sprouting, *vegfaa*

19   and *vegfab* have acquired specific regulatory elements that drive their expression in separate

20   domains, thereby locally influencing blood vessel formation.

21

22

23

1 **Mutant hindbrain phenotypes display cell number changes in particular blood vessels**

2 Angiogenesis requires the coordination of endothelial cell migration and proliferation (Adams

3 and Alitalo, 2007; Hogan and Schulte-Merker, 2017; Potente et al., 2011; Schuermann et al.,

4 2014). We therefore set out to investigate the influence of either *vegfa* gene on these processes.

5 To do so, we quantified cell numbers using the double transgenic line *Tg(kdrl:Hsa.HRAS-*

6 *mCherry)s916*; *Tg(fli1a:nEGFP)y7,* in which EC nuclei contain EGFP protein and membranes are

7 labelled by virtue of mCherry expression (Hogan et al., 2009; Roman et al., 2002). After

8 completion of BA and CtA sprouting (58 hpf time point), both mutants displayed lower total cell

9 numbers when compared to wildtype (wt) embryos (Figure 1Q-T). Further analysis revealed that

10 neither *vegfaamu128* nor *vegfabmu155* affected PHBC cell numbers (Figure 1U). As expected, BA

11 cell numbers were specifically affected in *vegfabmu155* mutants (Figure 1V). The amounts of CtAs

12 decreased about 50% in *vegfaa* mutants (Figure 1R, quantified in Figure 1P) and accordingly,

13 total CtA cell numbers were also reduced in these mutants (Figure 1W). Surprisingly however,

14 total CtA cell numbers were similarly decreased in *vegfab* mutants when compared to wt

15 embryos (Figure 1W), even though *vegfabmu155* mutants formed normal numbers of CtAs (Figure

16 1P). We therefore reasoned that *vegfab* might affect EC numbers in individual CtAs. Indeed,

17 while individual CtAs in *vegfaamu128* mutants contained similar quantities of ECs compared to wt

18 embryos, cell numbers per CtA in *vegfabmu155* were significantly decreased (Figure 1X). Thus,

19 *vegfab* specifically influenced EC numbers in blood vessel sprouts without affecting their

20 growth. These findings suggest that the two zebrafish *vegfa* paralogs not only differentially affect

21 blood vessel formation due to their distinct gene expression domains, but that they might also

22 have acquired separate biological functions.

23

1 **Vegfab signalling is specifically required for EC proliferation**

2 To test this hypothesis, we leveraged the accessibility of zebrafish for time lapse imaging. We

3 used *Tg(kdrl:Hsa.HRAS-mCherry)*$_{s916}$; *Tg(fli1a:nEGFP)*$_{y7}$ embryos to track the proliferative

4 behaviours of individual ECs. In wt embryos, we observed CtA EC proliferation between 32 and

5 42 hpf (Figure S1E, white dots; Video S4). Ultimately, 16.5 % of CtA cells were derived from a

6 cell division (Figure S1H, I). Although fewer CtAs sprouted in *vegfaa*$_{mu128}$ mutants, the ones that

7 formed displayed a similar percentage of CtA cells derived from proliferation when compared to

8 wt embryos (Figure S1F, white dots, quantified in Figure S1H, I; Video S5). By contrast,

9 *vegfab*$_{mu155}$ mutants showed a reduction of cells derived from proliferation to 3.4 % (Figure S1G,

10 white dots, quantified in Figure S1H, I; Video S6). Thus, *vegfaa* signalling cannot compensate

11 for loss of *vegfab* signalling in stimulating EC proliferation during CtA sprouting. Together,

12 these findings suggest that *vegfab* signalling might be critically required in controlling EC

13 proliferation.

14

15 **VEGFab and VEGFaa differentially affect intersegmental blood vessel sprouting**

16 To corroborate our findings, we analyzed the morphology of intersegmental blood vessels

17 (ISVs), the first blood vessels that form via angiogenesis in zebrafish embryos (Isogai et al.,

18 2003). In wt embryos, ISVs sprout from the dorsal aorta and anastomose in the dorsal region of

19 the zebrafish trunk at 30 hpf (Isogai et al., 2003) (Figure S2A, B, quantified in Figure S2K).

20 *vegfaa*$_{mu128}$ heterozygous embryos showed a variable degree of stalled ISVs (Figure S2C, D,

21 arrowhead, quantified in Figure S2K), indicating haploinsufficiency, as previously reported for

22 VEGFA mutant mice (Carmeliet et al., 1996). ISVs failed to form in *vegfaa*$_{mu128}$ homozygous

23 embryos (Figure S2E, F, quantified in Figure S2K), as shown earlier for independently generated

8

1 *vegfaa* mutants (Rossi et al., 2016). Surprisingly, neither *vegfab_mu155* heterozygous nor

2 homozygous mutants showed defects in ISV morphology at 30 hpf (Figure S2G-J, quantified in

3 Figure S2K). These results thus underscore a conserved role of *vegfaa* signaling during ISV

4 formation, while *vegfab* appears to be dispensable during this process.

5 Motivated by our observations concerning the specific functions of *vegfaa* and *vegfab* in

6 CtA formation, we set out to determine whether *vegfab* might similarly affect EC proliferation in

7 ISV ECs. As previously reported, wt embryos contained either 3 or 4 cells per ISV (Figure 2A,

8 B, quantified in Figure 2G), (Childs et al., 2002; Costa et al., 2016; Siekmann and Lawson,

9 2007). ISVs in heterozygous *vegfaa_mu128* mutants contained significantly fewer endothelial cells

10 (Figure 2C, D, quantified in Figure 2G). *Vegfab_mu155* mutants displayed a reduction in ISV EC

11 numbers (Figure 2E, F, quantified in Figure 2G) without obvious sprouting defects. Thus, similar

12 to brain CtAs, loss of *vegfab* specifically reduces ISV cell numbers.

13 We then set out to analyze how *vegfaa* and *vegfab* might affect endothelial cell migration

14 and proliferation. To do so, we performed time-lapse imaging of Tg*(kdrl:Hsa.HRAS-*

15 *mCherry)s916*; *Tg(fli1a:nEGFP)y7* double transgenic zebrafish embryos. As determined by nuclear

16 displacement, wt tip cells on average migrated about 100 um within 6 h (Figure 2H, arrowheads,

17 quantified in Figure 2L; Video S7), as previously reported (Costa et al., 2016). By contrast, ISVs

18 in *vegfaa_mu128* heterozygous fish displayed two different behaviors: Tip cells either migrated

19 similar to wt cells (Figure 2I, quantified in Figure 2L; Video S8), or showed severe migration

20 defects with tip cells stalling midway along the somite (Figure 2J, quantified in Figure 2L; Video

21 S9). Therefore, lack of one *vegfaa* allele can differentially affect individual ISVs. *Vegfab*

22 homozygous mutants showed a decrease in cell migration in the midway position, but later

23 recovered and reached the dorsal region of the embryo at the same time as the wildtype cells did

9

1   (Figure 2K, quantified in Figure 2L; Video S10). Therefore, absence of *vegfaa* signaling can

2   have pronounced effects on EC migration, while *vegfab* mutants show only minor cell migration

3   defects.

4   By contrast, EC proliferation was strongly affected in *vegfaa* and *vegfab* mutants. Time-

5   lapse imaging revealed that in wt embryos each ISV showed around one EC proliferation event

6   (Figure 2M, quantified in Figure 2P; Video S11). This was reduced to about half for both

7   *vegfaa_{mu128}* (Figure 2N, quantified in Figure 2P; Video S12) and *vegfab_{mu155}* (Figure 2O,

8   quantified in Figure 2P; Video S13) mutants. To further investigate the influence of *vegfab* on

9   EC proliferation, we globally overexpressed Vegfab via mRNA injection. This led to an increase

10   in EC numbers within ISVs without affecting their overall morphology (Figure S3). In summary,

11   our findings suggest that *vegfaa* signaling drives EC migration and proliferation, while *vegfab*

12   signaling mainly affects EC proliferation.

13

14   **Vegfab controls EC proliferation independently of ERK signaling**

15   We reasoned that the observed differences in EC behaviors between *vegfaa_{mu128}* and *vegfab_{mu155}*

16   mutants might enable us to dissect out signaling pathways downstream of VEGFA that

17   specifically control proliferation. Previous studies implicated signaling through MAPK/ERK in

18   influencing EC proliferation (Claesson-Welsh, 2016; Simons et al., 2016). We therefore set out

19   to determine potential changes in ERK phosphorylation in *vegfab* mutants. Surprisingly, pERK

20   antibody staining in ISVs was unchanged in *vegfab* mutant embryos (Figure 3A, B, quantified in

21   Figure 3C). ERK signaling furthermore influences gene expression patterns within ISVs (Shin et

22   al., 2016). We did not detect changes in either of the two reported ERK downstream genes *dll4*

23   (Figure 3D-G) or *flt4* (Figure 3H-K) in *vegfab_{mu155}* mutants. Lastly, treating wt embryos with

1   phorbol 12-myristate 13-acetate (PMA), which increased ERK phosphorylation (Figure S4), did

2   not change EC numbers within ISVs (Figure 3L-Q, quantified in Figure 3X). PMA treatment

3   also failed to rescue EC numbers in *vegfab_mu155* mutants (Figure 3R-W, quantified in Figure 3X).

4   Therefore, ERK signaling does not play a major role downstream of *vegfab* signaling in

5   controlling EC proliferation in ISVs.

6

7   **Loss of PI3K signaling specifically affects endothelial cell proliferation**

8   We next focused on PI3K signaling, as another important pathway downstream of VEGFA

9   signaling (Graupera and Potente, 2013). Treating zebrafish embryos with 10 um of the PI3K

10   inhibitor LY294002 (Vlahos et al., 1994) reduced phosphorylation of the PI3K downstream

11   kinase AKT without affecting gross embryonic morphology (Figure S5). ISV morphology was

12   unaffected when treating zebrafish embryos from 22 to 32 hpf (Figure 4A, D). However, similar

13   to *vegfab_mu155* mutants, EC numbers were significantly reduced in inhibitor treated embryos

14   when compared to DMSO treated control embryos (Figure 4B, C, E, F, quantified in Figure 4G).

15   We then investigated whether this reduction in cell numbers was due to the reported effects of

16   PI3K signaling on cell migration. Surprisingly, time-lapse imaging of developing ISVs did not

17   reveal changes in cell migration upon LY294002 treatment (Figure 4H, I, quantified in Figure 4J;

18   Videos S14 and 15). We therefore investigated EC proliferation in inhibitor treated embryos.

19   This analysis revealed that blocking PI3K signaling led to a decrease in proliferation events

20   (Figure 4K, L, quantified in Figure 4M; Videos S16 and S17). As LY294002 inhibits multiple

21   PI3K isoforms in addition to other kinases (Davies et al., 2000; Workman et al., 2010), we

22   investigated ISV formation after treating embryos with the PI3K p110 alpha isoform specific

23   inhibitor GDC-0326 (Heffron et al., 2016). GDC-0326 treatment effectively reduced AKT

1   phosphorylation at concentrations ranging from 10 um to 50 um (Figure S6A) and reduced ISV

2   cell numbers without affecting ISV morphology (Figure S6B-M, quantified in Figure S6N).

3   Thus, while not affecting ISV EC migration during short term inhibitor treatment, PI3K

4   signaling downstream of the 110 alpha isoform plays important roles in controlling EC

5   proliferation during developmental angiogenesis.

6

7   **Cdkn1a/p21 is a downstream target of vegfab/PI3K signaling in regulating EC**

8   **proliferation**

9   To identify *vegfab* target genes that might lead to altered proliferative behaviors, we used

10   Fluorescence-activated cell sorting (FACS) to sort GFP and mCherry positive ISV and arterial

11   ECs from *vegfab* morpholino injected embryos using a triple transgenic strategy (Figure 5A). We

12   then analyzed expression of genes implicated in cell cycle regulation. This analysis revealed

13   mRNA upregulation of the negative cell cycle regulator *cdkn1a/p21* in ECs of *vegfab*

14   morpholino injected embryos (Figure 5B). We furthermore determined the influence of PI3K

15   inhibition on Cdkn1a/p21 protein expression in cultured human umbilical vein endothelial cells

16   (HUVEC). Overall Cdkn1a/p21 protein levels were unchanged after LY294002 treatment

17   (Figure 5C). However, we detected a striking change in Cdkn1a/p21 protein localization from

18   cytoplasmic towards nuclear (Figure 5D-I, quantified in Figure 5J). Nuclear localization has been

19   implicated in mediating the cell growth inhibiting function of Cdkn1a/p21 (Zhou et al., 2001).

20   Thus, both *vegfab* and PI3K signaling can influence the abundance and localization of

21   Cdkn1a/p21 in ECs.

22   Based on these findings, we investigated whether knocking down Cdkn1a/p21 could

23   rescue the proliferation defects observed upon loss of *vegfab* or PI3K signaling. Injection of

12

1   Cdkn1a/p21 morpholino into wt embryos caused a mild increase in ISV EC numbers (Figure 6A,

2   B, quantified in Figure 6E). Injecting Cdkn1a/p21 morpholinos into *vegfab$_{mu155}$* mutants led to a

3   rescue of EC numbers back to wt levels (Figure 6C, D, quantified in Figure 6E). Similarly,

4   injection of Cdkn1a/p21 morpholino prior to PI3K inhibitor treatment increased ISV EC

5   numbers back to wt levels (Figure 6F-I, quantified in Figure 6J). Therefore, reducing

6   Cdkn1a/p21 levels can rescue the proliferation defects observed upon loss of *vegfab* and PI3K

7   signaling.

8

9   **Inhibition of PI3 kinase signaling during retinal angiogenesis reduces endothelial cell**

10   **proliferation**

11   To investigate whether PI3K signaling influences EC proliferation in other angiogenic settings,

12   we analyzed blood vessel development in the mouse retina. Here, new blood vessels sprout from

13   the optic nerve towards the periphery of the retina after birth. Intraperitoneal injection of the

14   PI3k 110 alpha subunit-specific inhibitor GDC-0941 effectively reduced AKT phosphorylation

15   in ECs after 24 h of treatment, as analyzed in lung lysates from P6 mice (Figure S7A). It

16   furthermore reduced the phosphorylation of S6 kinase, a downstream target of PI3K signaling

17   (Chung et al., 1994) (Figure S7B-E). Incorporation of EdU was strongly reduced in inhibitor

18   treated embryos, both at the angiogenic front (Figure 7A-D, quantified in G) and in the vein

19   region of the retina (Figure 7E, F, quantified in H), where ECs continue to proliferate. Thus,

20   similar to our observations in zebrafish embryos, PI3K signaling affects endothelial cell

21   proliferation during mouse retinal angiogenesis.

22

23

1   **DISCUSSION**

2   Tissue vascularization requires coordinated cellular responses to growth factors, such as

3   Vegfa, in order to generate appropriate amounts of new ECs, allow them to sprout into avascular

4   areas and ultimately differentiate into the correct numbers of arteries, capillaries and veins. How

5   a single ligand can control the multitude of cellular responses necessary to achieve these tasks is

6   an outstanding question in the field. Our work on the duplicated Vegfa ligands in zebrafish

7   identifies a specific function of PI3 kinase signaling in response to ECM bound *vegfab* ligands in

8   regulating EC proliferation. This was an unexpected discovery, since signaling through

9   MAPK/ERK was thought to be the main driver of EC proliferation downstream of Vegfa

10   signaling (Koch and Claesson-Welsh, 2012; Meadows et al., 2001; Simons et al., 2016;

11   Srinivasan et al., 2009; Takahashi et al., 1999). What might be the reason for this discrepancy?

12   So far, animal models carrying mutations in components of the Vegf pathway showed

13   simultaneous defects in EC proliferation and migration. For instance, zebrafish mutants in *kdrl*,

14   *plcg* or treated with the Vegf pathway inhibitor SU5416 display an absence of ERK

15   phosphorylation (Fish et al., 2017; Shin et al., 2016), together with a reduction in ISV outgrowth

16   and cell numbers. Similarly, mutants in *vegfaa* show a severe reduction in EC numbers and

17   migration during ISV formation (Jin et al., 2017), phenotypes also seen in *VEGFA* mutant mice

18   (Carmeliet et al., 1996; Ferrara et al., 1996). Therefore, it has been difficult in animal models to

19   dissect out the individual contribution of a given gene or its downstream pathway components to

20   either process.

21   Specific manipulations of ERK signaling in cultured ECs showed a requirement for DNA

22   synthesis downstream of VEGFR2 activation, a process that was independent of PI3K activity

23   (Takahashi et al., 1999). However, deletion of ERK1 in mice did not result in vascular

14

1   phenotypes (Pages et al., 1999), while knocking out ERK2 specifically in ECs in an ERK1-/-

2   background affected EC migration and proliferation (Srinivasan et al., 2009). Our study together

3   with the study of Shin et al. (Shin et al., 2016) suggests that in developing ISVs, ERK signaling

4   rather controls EC migration instead of proliferation. A similar specific influence of ERK

5   signaling on migration was reported in a HUVEC tube formation assay and for tumor ECs

6   (Mavria et al., 2006). These results suggest that ERK phosphorylation can influence EC

7   migration and/or proliferation depending on the developmental setting and the EC type analyzed.

8   Our work points towards a critical role of PI3K signaling for EC proliferation during ISV

9   outgrowth. We find that blocking PI3K using different inhibitors selectively prevented ISV EC

10   proliferation without influencing cell migration. This is in contrast to previous studies showing

11   that PI3K signaling specifically affected EC migration in developing mouse embryos and in

12   cultured ECs, with only minor effects on EC proliferation (Graupera et al., 2008; Takahashi et

13   al., 1999). A previous study in zebrafish ISVs also showed that blocking PI3K signaling using

14   the LY294002 inhibitor affected cell migration without reducing EC proliferation (Nicoli et al.,

15   2012). We directly imaged dividing cells using time-lapse imaging, while Nicoli et al.

16   determined differences in BrdU incorporation. It might therefore be that PI3K signaling is

17   important for cytokinesis with less effects on DNA synthesis, as previously shown in

18   *Dictyostelium discoideum* cells (Janetopoulos et al., 2005). In addition, differences in the

19   duration of PI3K inhibition will affect EC behaviors. We blocked PI3K signaling for 10 hours,

20   while Graupera et al. analyzed vascular phenotypes after several days of removing PI3K

21   110alpha kinase function from ECs (Graupera et al., 2008).

22   Other studies have shown that PI3K signaling downstream of VEGF receptor signaling

23   can lead to an increase in EC proliferation. Dayanir et al. generated a chimeric VEGF receptor 2

15

1 that could be activated using CSF-1 (Dayanir et al., 2001). When PI3K signaling was

2 compromised, CSF-1 stimulation of this receptor failed to induce EC proliferation. Another

3 study showed that Y1212 in VEGFR2 was important to control PI3K signaling pathway

4 activation upstream of myc-dependent EC proliferation (Testini et al., 2019). In line with our

5 observations in the mouse retina, blocking PI3K signaling in this setting reduced the number of

6 phospho-histone 3 positive ECs (Ola et al., 2016) and led to a reduction in EdU incorporation

7 (Angulo-Urarte et al., 2018). Importantly, activating mutations in PIK3CA can lead to venous

8 malformations that are characterized by increased EC proliferation (Castel et al., 2016; Castillo

9 et al., 2019; Castillo et al., 2016). Together, these studies suggest a more important role of PI3K

10 signaling in controlling EC proliferation downstream of Vegf signaling than previously

11 anticipated. However, further work will be necessary to precisely determine in which EC

12 populations and at which stages of the cell cycle PI3K signaling is required. Of note, we still

13 observed EC proliferation in PI3K inhibitor treated or *vegfab* mutant embryos, suggesting the

14 existence of other signaling pathways contributing to ISV EC proliferation.

15   Why are Vegfab ligands specifically affecting PI3K signaling and EC proliferation

16 without a major influence on EC migration? One reason for this might due to the existence of

17 differentially spliced Vegfa isoforms. In other species, all Vegfa isoforms are being generated by

18 the same gene, while in zebrafish only *vegfaa* can generate both short and long, ECM binding,

19 isoforms (Bahary et al., 2007). *Vegfab* exclusively generates ECM binding isoforms. This setting

20 allowed us to determine the unique effects of ECM binding Vegfa isoforms on EC behaviors

21 during embryogenesis. Previous studies in developing mice (Ruhrberg et al., 2002; Stalmans et

22 al., 2002), disease settings (Brash et al., 2019; Cheng et al., 1997; Guo et al., 2001; Kazemi et al.,

23 2016) and in cultured ECs (Chen et al., 2010; Delcombel et al., 2013; Fearnley et al., 2016;

1   Herve et al., 2005; Park et al., 1993; Shiying et al., 2017) carefully investigated the effects of the

2   different VEGF isoforms on cellular behaviors (for review see (Peach et al., 2018; Woolard et

3   al., 2009)). Some studies suggested that there are no differences in the ability of various VEGFA

4   isoforms to support EC proliferation (Ruhrberg et al., 2002), while others showed that ECs

5   cultured on ECM derived from cells expressing VEGF189 or VEGF206 proliferated more

6   strongly than those cultured in the presence of VEGF165 (Park et al., 1993). Our studies support

7   the latter findings by showing that matrix bound Vegfab isoforms stimulate EC proliferation. We

8   furthermore find that EC proliferation in *vegfab$_{mu155}$* mutants is more strongly affected in actively

9   sprouting ECs in the forming CtAs and ISVs. We hypothesize that this might be due to the fact

10   that during angiogenic growth ECs degrade the ECM, possibly releasing bound VEGF

11   molecules, which would make them available to the invading ECs. Thus, the ability of long

12   VEGF isoforms to associate with the ECM could provide a readily available growth factor pool

13   within tissues.

14   Cell cycle regulation is a key prerequisite for proper embryonic development and tissue

15   homeostasis and is regulated by a stoichiometric competition between proliferation promoting

16   cyclinD expression that is induced by mitogens and inhibitory cdkn1a/p21 (Pack et al., 2019).

17   Previous work showed that cdkn1a/p21 levels vary between cells in a given population and that

18   these levels can determine the proportion of cells that actively cycle (Overton et al., 2014).

19   Furthermore, increased levels of cdkn1a/p21 after mitosis can lead to cellular quiescence, while

20   cells with lower cdkn1a/p21 levels continue to proliferate (Spencer et al., 2013). A similar

21   balance of cdkn1a/p21 might control the number of proliferating ECs during ISV sprouting.

22   Indeed, when comparing different ISVs, we observe a variation in proliferating ECs. In

23   cdkn1a/p21 knockdown embryos, a greater number of ECs proliferate, while a reduction in

1   *vegfab* signaling increases expression of cdkn1a/p21 and causes fewer ECs to proliferate.

2   Recently, increases in ERK signaling were shown to upregulate cdkn1a/p21 expression in ECs in

3   the mouse retina, resulting in cell cycle arrest (Pontes-Quero et al., 2019). Our results suggest

4   that PI3K signaling downstream of *vegfab* similarly controls the amount and/or localization of

5   cdkn1a/p21, thereby determining the amount of actively cycling ECs during angiogenesis.

6   Of note, cdkn1a/p21 can also influence cell migration via the inhibition of Rho/ROCK

7   (Rho-associated kinase) signaling (Kreis et al., 2019; Tanaka et al., 2002). During tumorigenesis,

8   upregulation of cdkn1a/p21 can induce growth arrest, allowing breast cancer cells to become

9   more migratory and invasive (Qian et al., 2013). Previous studies showed that activation of the

10 PI3K target Akt results in cdkn1a/p21 cytoplasmic localization, releasing cdkn1a/p21's growth

11 inhibiting function (Zhou et al., 2001). Our results show a similar effect of PI3K signaling on

12 cdkn1a/p21localization in ECs. Therefore, proper activation of PI3K signaling upstream of

13 cdkn1a/p21 might be important for controlling the switch between EC migration and

14 proliferation. A better understanding of the mechanisms controlling this switch will further our

15 understanding of tissue morphogenesis and help to manipulate aberrant blood vessel

16 development in beneficial ways.

17

18 **MATERIALS AND METHODS**

19 **Zebrafish strains**

20 Zebrafish were maintained as described previously (Westerfield, 1993). Transgenic lines and

21 mutants used were *Tg(kdrl:EGFP)s843, Tg(kdrl:Hsa.HRAS-mCherry)s916, Tg(fli1a:nEGFP)y7,*

22 *Tg(dll4:gal4)mu106, Tg(UAS:GFP)nkuasgfp1a, vegfaamu128* (this study), *vegfabmu155* (this study).

23 References for zebrafish transgenic lines can be obtained on zfin.org. Adult zebrafish used in this

1   study to generate embryos were between 1-2 years of age. Embryos were not selected for gender.

2   All animal experiments were performed in compliance with the relevant laws and institutional

3   guidelines and were approved by local animal ethics committees of the Landesamt für Natur,

4   Umwelt und Verbraucherschutz Nordrhein-Westfalen.

5

6   **Morpholino injections and drug treatment**

7   Morpholinos were obtained from Gene-Tools and dissolved in distilled water. Morpholinos

8   (MOs) targeting *cdkn1a/p21* (3 ng/embryo) (Sidi et al., 2008), *vegfab* (5 ng/ embryo) (Bahary et

9   al., 2007) and a standard control MO (Hasan et al., 2017) have been described previously. To

10 inhibit PI3K, embryos were dechorionated and incubated in 10 uM LY-294002 hydrochloride

11 (SIGMA) for 10 hours prior to imaging. To specifically inhibit PI3K 110 alpha, embryos were

12 dechorionated and incubated in 10 uM, 25 uM or 50 uM of GDC-0326 (Cayman Chemical). To

13 activate ERK signalling, embryos were dechorionated and incubated in 0.25 uM Phorbol-12-

14 myristat-13-acetate (PMA) (SIGMA) for 4 hours prior to imaging.

15

16 **Live imaging, confocal microscopy and image processing**

17 For *in vivo* imaging, live embryos were mounted in 1 % or 1.5 % low-melting-point agarose in

18 E3 embryo medium with 168 mg l$_{-1}$ tricaine (1x) for anaesthesia and 0.003 % phenylthiourea to

19 inhibit pigmentation. Imaging was carried out on an inverted Leica SP5, SP8 or a Zeiss LSM780

20 confocal microscope using a 20× dry objective. A heated microscope chamber at 28.5 °C was

21 used for recording time-lapse videos. Stacks were taken every 15-20 min with a step size of

22 2 um. Confocal stacks and time-lapse videos were analysed using IMARIS Software (Bitplane).

23

1   **Fluorescence-activated cell sorting (FACS) of arterial ECs from zebrafish embryos**

2   Arterial ECs were obtained from triple-transgenic zebrafish embryos, in which

3   *Tg(kdrl:Hsa.HRAS-mCherry)$_{s916}$* exhibits pan-endothelial expression, and the combination of

4   *Tg(dll4:gal4)$_{mu106}$*; *(UAS:GFP)$_{nkuasgfp1a}$* labels arterial ECs within this population. Embryos were

5   deyolked in calcium free Ringer's solution and treated with 0.5% Trypsin-EDTA (Gibco, 15400-

6   054) containing 50 mg/ml collagenase Type IV (Gibco,17104-019) and dissociated by constant

7   pipetting. The reaction was stopped by adding 5% FBS and the cells were pelleted by

8   centrifugation. The pelleted cells were washed with 1x HBSS buffer (Gibco, 14185052) and

9   passed through 40-micron nylon filters. FACS was performed on the cell suspension for arterial

10 (mCherry+/GFP+) and the venous (mCherry+) cells at room temperature. Sorted cells were

11 collected in RLT buffer (Qiagen) for RNA isolation.

12

13 **Quantitative Polymerase Chain Reaction (qPCR)**

14 RNA was isolated with RNeasy Plus Micro kit (Qiagen) from whole zebrafish embryos or sorted

15 cells and reverse transcribed with iScript cDNA Synthesis Kit (BioRad). For qPCR, cDNA

16 produced from 15 ng RNA and 8 pmol of each forward and reverse primer per reaction and

17 Power SYBR Green PCR Master Mix (Applied Biosystems) were used. Relative expression was

18 quantified by ΔΔCt method using RPL13A as an endogenous control. The expression in control

19 sample (unsorted cells/ctr MO injected embryos) was set as 1. ΔCt values were used for

20 statistical analysis. The following primers were used:

21 Cdk2-fwd: 5' -CGGAGGGCACTGTTTCCTGGAG- 3'

22 Cdk2-rev: 5' -ACATTTGCCCAAGAAGGTCTCTGCC- 3'

23 Cdkn1a/p21-fwd: 5' -AGCTTCAGGTGTTCCTCAGCTCCT- 3'

1   Cdkn1a/p21-rev: 5' -CCGGCCCGAAAAGACTCCGC- 3'

2   Cdkn1b/p27-fwd: 5' -TACAGCCGATCGGAGCGGGG- 3'

3   Cdkn1b/p27-rev: 5' -TGACACGATGAGTCGAGACAGGAGC- 3'

4   RPL13A-fwd: 5' - TCTGGAGGACTGTAAGAGGTATGC

5   RPL13A-rev: 5' - AGACGCACAATCTTGAGAAGCAG

6

7   **Generation of *vegfaa$_{mu128}$* and *vegfab$_{mu155}$* mutant zebrafish**

8   Zinc-finger nucleases (ZFNs) against *vegfaa* were designed as previously described (Siekmann

9   et al., 2009). In the *vegfaa$_{mu128}$* allele, 7 nucleotides were deleted in exon 1 at the ZFN target site,

10 resulting in an early stop codon after 18 amino acids. TALEN mutagenesis targeting *vegfab* was

11 performed as described previously (Sugden et al., 2017). In the *vegfab$_{mu155}$* allele, 1 nucleotide

12 was deleted and 2 nucleotides were inserted in exon 1 at the TALEN target site. This resulted in

13 an early stop codon after 12 amino acids.

14

15 **Genotyping**

16 Primers for genotyping *vegfaa* were:

17 Vegfaa-fwd: 5' -GCTTTCTTAATTGTTTTGAGAGCCAG- 3'

18 Vegfaa-rev: 5' –GGTGTGGGCTATTGCATTTC- 3'

19 PCR products were digested with BccI (NEB). Fragment sizes are 116 bp + 123 bp for wild type

20 allele and 239 bp for *vegfaa$_{mu128}$* allele.

21 Primers for genotyping vegfab were:

22 Vegfab-fwd: 5' -GGACCAACATGGGATTCTTG- 3'

23 Vegfab-rev: 5' -GGGTGGTCAGATATGCTCGT- 3'

1   PCR products were digested with BsrI (NEB). Fragment sizes are 188 bp + 221 bp for wild type

2   allele and 409 bp for *vegfabmu155* allele.

3

4   **Cloning of *vegfab171* and overexpression studies**

5   *Vegfab171* was amplified with primers

6   VEGFabattB1 ggggacaagtttgtacaaaaaagcaggctGTTAAAAACGGGCAACGGCGG and

7   VEGFab attB2 ggggaccactttgtacaagaaagctgggtTCACCTCCTTGGTTTGTCACATCTGC

8   from zebrafish 24 hpf cDNA. cDNA was generated using RNA that was isolated with RNeasy

9   Plus Micro kit (Qiagen) from whole zebrafish embryos and reverse transcribed with iScript

10   cDNA Synthesis Kit (BioRad). BP reaction was performed according to the manufacturer's

11   instructions (ThermoFisher). Clones were verified by sequencing. *Vegfab* was then transferred

12   into pCSDest (Villefranc et al., 2007) using LR cloning (ThermoFisher). Plasmid DNA was

13   digested using NotI (NEB) and mRNA was generated using mMessage machine in vitro

14   transcription kit (ThermoFisher). 50 pg of mRNA was injected into 1-cell stage zebrafish

15   embryos.

16

17   **In situ hybridization and fluorescence in situ hybridizations (FISH) with antibody staining**

18   Whole-mount in situ hybridization was performed as previously described (Thisse and Thisse,

19   2008). Whole mount FISH combined with EGFP antibody staining was performed in

20   *Tg(kdrl:EGFP)s843* line as described previously (Kochhan and Siekmann, 2013). Previously

21   described probes were for *vegfaa* (Lawson et al., 2002), *vegfab* (Bahary et al., 2007), *dll4*

22   (Siekmann and Lawson, 2007), *flt4* (Lawson et al., 2001).

23

22

1   **Western blotting of zebrafish proteins**

2   Dechorionated zebrafish embryos were de-yolked in Ginzburg buffer (55 mM NaCl, 1.8 mM

3   KCl, 1.25 mM NaHCO3) and lysed in Laemli buffer (20 embryos in 80 ul). Either 10 or 20 ul of

4   sample were separated by 12 % SDS-PAGE and transferred onto PVDF membrane (Millipore).

5   After blocking with 5 % Milk powder (Roth) in TBST, membranes were incubated with anti-

6   phospho-p44/42 MAPK (Thr202/Tyr204) (1:1000; #8544; Cell Signaling), anti-p44/42 MAPK

7   antibody (1:2000; #9102, Cell Signaling) and anti-αActin antibody (1:5000; A-5060, Sigma),

8   Phospho-Akt (Ser473) (1:2000; #4060; Cell Signaling), Akt (1:1000; #9272; Cell Signaling).

9   Primary antibodies were detected using mouse IgG HRP linked whole Ab (1:4000; NXA931; GE

10   healthcare).

11

12   **Immunostaining of zebrafish embryos**

13   Immunostaining for phospho-p44/42 MAPK was performed as described previously (Costa et

14   al., 2016).

15

16   **Mouse retina**

17   To inhibit PI3K signaling, Pictilisib (GDC-0941, Selleckchem) stock solution was prepared by

18   dissolving 8.5 mg of powder in 63 ul DMSO. Before injection, 10 ul of the stock solution was

19   diluted in 190 ul of corn oil to get a final concentration of 6,8 ug/ul. 25 ul of this solution (or

20   vehicle only) was injected IP into each pup at P5 (55 mg/kg) and again 16 h later, before

21   collecting the tissues at P6 (injections at -24 h and -8 h time points). To detect proliferating cells

22   actively synthesizing DNA, EdU (Invitrogen - A10044) was injected IP 4 h before sacrifice; the

23   signal was developed with the Click-it EdU Alexa Fluor 647 Imaging Kit.

23

1 **Immunohistochemistry of mouse retinae**

2 For mouse retina immunostaining, eyes were collected at the indicated time points and fixed in

3 4% PFA in PBS for 1h at room temperature (RT). After two PBS washes, retinas were micro-

4 dissected and stained as described previously (Pontes-Quero et al., 2019). Briefly, retinas were

5 blocked and permeabilized with 0.3% Triton X-100, 3% FBS and 3% donkey serum in PBS.

6 Samples were then washed twice in PBLEC buffer (1 mM $CaCl_2$, 1 mM $MgCl_2$, 1 mM $MnCl_2$

7 and 1% Triton X-100 in PBS). Biotinylated isolectinB4 (Vector Labs, B-1205, diluted 1:50) or

8 primary antibodies (see below) were diluted in PBLEC buffer and tissues were incubated in this

9 solution for 2 h at RT or overnight at 4ºC. After five washes in blocking solution diluted 1:2,

10 samples were incubated for 1 h at RT with Alexa-conjugated secondary antibodies (Molecular

11 Probes). After two washes in PBS, retinas were mounted with Fluoromount-G

12 (SouthernBiotech). To detect EdU-labelled DNA, an additional step was performed before

13 mounting using the Click-It EdU kit (Thermo Fisher, C10340). Primary antibodies were used

14 against the following proteins: Erg (AF-647, Abcam ab196149, 1:100), Phospho-S6 Ribosomal

15 Protein (Ser235/236) (Cell Signalling Ab #4856, 1:100). The following secondary antibodies

16 were used: Donkey anti-rabbit Cy3 (1:400, 711-167-003, Jackson Immunoresearch) and

17 Streptavidin Alexa 405 (1:400, S-32351, Thermofisher).

18

19 **Western blot analysis of mouse proteins**

20 For the analysis of protein expression, dissected organs were transferred to a reagent tube and

21 frozen in liquid nitrogen. On the day of the immunoblotting the tissue was lysed with lysis buffer

22 [(Tris-HCl pH=8 20 mM, EDTA 1 mM, DTT 1 mM, Triton X-100 1% and NaCl 150 mM,

23 containing protease inhibitors (P-8340 Sigma) and phosphatase inhibitors (Calbiochem 524629)

1   and orthovanadate-Na 1 mM)] and homogenized with a cylindrical glass pestle. Tissue/ cell

2   debris was removed by centrifugation, and the supernatant was diluted in loading buffer and

3   analyzed by SDS–PAGE and immunoblotting. Membranes were blocked with BSA and

4   incubated with primary antibodies diluted 1/1000 against Cdh5/VE-cadherin (BD Biosciences

5   555289), Phospho-Akt (Cell Signalling, #4060S), Akt (Cell Signaling #9272S) or β-Actin

6   (Santa Cruz Biotechnologies, sc-47778).

7

8   **Microscopy of mouse retina**

9   We used a Leica TCS SP8 confocal with a 405 nm laser and a white laser that allows excitation

10   at any wavelength from 470nm to 670nm. All images shown are representative of the results

11   obtained for each group and experiment. Littermates were dissected and processed under exactly

12   the same conditions. Comparisons of phenotypes or signal intensity were made with pictures

13   obtained using the same laser excitation and confocal scanner detection settings. Images were

14   processed using ImageJ/Fiji and Adobe Photoshop.

15

16   **Quantitative analysis of retinal vasculature**

17   Single low magnification (10x lens) confocal fields of immunostained retinas were quantified

18   with Fiji/ImageJ. Each microscopy field contained hundreds of ECs, and the relative or absolute

19   number of cells in each field is indicated in the charts by a dot. As indicated in figure legends,

20   microscopy images from several animals and retinas were used for the phenotypic comparisons

21   and quantifications. Vascular IsolectinB4+ area and Erg+ or Edu+ cells were quantified

22   semiautomatically using custom Fiji macros. Endothelial cell density (EC number/mm2) was

23   measured as the number of Erg+ cells relative to the vascularized IsolectinB4+ area in each field.

1   The frequencies of Erg+ cells (ECs) in S-phase (EdU+) was determined as the ratio of double-

2   positive cells to the total number of Erg+ cells per field.

3

4   **Statistical analysis**

5   Two groups of samples with a Gaussian distribution were compared by unpaired two-tailed

6   Student *t*-test. Comparisons among more than two groups were made by ANOVA followed by

7   the Turkey pairwise comparison. Column statistics were performed on data sets to check for

8   normal distribution and appropriate tests to determine significance were performed using the

9   Prism7 software. Each experiment was performed at least three times. Graphs represent mean +/-

10 SD as indicated, and differences were considered significant at $p < 0.05$. All calculations were

11 done in Excel and final datapoints analyzed and represented with GraphPad Prism. The sample

12 size was chosen according to the observed statistical variation and published protocols. The

13 experiments were not randomized, investigators were not blinded to allocation during

14 experiments and outcome assessment and sample sizes were not predetermined.

15

16 **MATERIALS AVAILABILITY**

17 All reagents and zebrafish lines generated in this study are available from the Lead Contact with

18 a completed Materials Transfer Agreement.

19

20 **ACKNOWLEDGEMENTS**

26

9

10 **AUTHOR CONTRIBUTIONS**

11 M.L. and A.F.S. conceived the experiments and analyzed the data. A.F.S. supervised the work.

12 M.L. analyzed *vegfaa* and *vegfab* mutants, performed drug treatmens, pERK stainings and p21

13 knockdown experiments. M.L. also performed all cell culture experiments. A.F.S. cloned *vegfab*

14 and performed overexpression experiments. N.O. generated the *vegfaa* and *vegfab* mutants. E.L.

15 performed FACS of zebrafish endothelial cells and qPCR experiments. D.H. analyzed data.

16 S.F.R. performed mouse retina experiments and analyzed data. R.B. analyzed data of mouse

17 retina. All authors discussed experiments and commented on the manuscript.

18

19 **REFERENCES**

20 Adams, R.H., and Alitalo, K. (2007). Molecular regulation of angiogenesis and lymphangiogenesis. Nat Rev Mol
21 Cell Biol *8*, 464-478.
22 Alvarez-Aznar, A., Muhl, L., and Gaengel, K. (2017). VEGF Receptor Tyrosine Kinases: Key Regulators of
23 Vascular Function. Curr Top Dev Biol *123*, 433-482.
24 Angulo-Urarte, A., Casado, P., Castillo, S.D., Kobialka, P., Kotini, M.P., Figueiredo, A.M., Castel, P., Rajeeve, V.,
25 Mila-Guasch, M., Millan, J*., et al.* (2018). Endothelial cell rearrangements during vascular patterning require PI3-
26 kinase-mediated inhibition of actomyosin contractility. Nature communications *9*, 4826.
27 Bahary, N., Goishi, K., Stuckenholz, C., Weber, G., Leblanc, J., Schafer, C.A., Berman, S.S., Klagsbrun, M., and
28 Zon, L.I. (2007). Duplicate VegfA genes and orthologues of the KDR receptor tyrosine kinase family mediate
29 vascular development in the zebrafish. Blood *110*, 3627-3636.

1   Bowler, E., and Oltean, S. (2019). Alternative Splicing in Angiogenesis. Int J Mol Sci *20*.
2   Brash, J.T., Denti, L., Ruhrberg, C., and Bucher, F. (2019). VEGF188 promotes corneal reinnervation after injury.
3   JCI Insight *4*.
4   Bussmann, J., Wolfe, S.A., and Siekmann, A.F. (2011). Arterial-venous network formation during brain
5   vascularization involves hemodynamic regulation of chemokine signaling. Development *138*, 1717-1726.
6   Carmeliet, P., Ferreira, V., Breier, G., Pollefeyt, S., Kieckens, L., Gertsenstein, M., Fahrig, M., Vandenhoeck, A.,
7   Harpal, K., Eberhardt, C., *et al.* (1996). Abnormal blood vessel development and lethality in embryos lacking a
8   single VEGF allele. Nature *380*, 435-439.
9   Carmeliet, P., Ng, Y.S., Nuyens, D., Theilmeier, G., Brusselmans, K., Cornelissen, I., Ehler, E., Kakkar, V.V.,
10 Stalmans, I., Mattot, V., *et al.* (1999). Impaired myocardial angiogenesis and ischemic cardiomyopathy in mice
11 lacking the vascular endothelial growth factor isoforms VEGF164 and VEGF188. Nat Med *5*, 495-502.
12 Castel, P., Carmona, F.J., Grego-Bessa, J., Berger, M.F., Viale, A., Anderson, K.V., Bague, S., Scaltriti, M.,
13 Antonescu, C.R., Baselga, E., *et al.* (2016). Somatic PIK3CA mutations as a driver of sporadic venous
14 malformations. Science translational medicine *8*, 332ra342.
15 Castillo, S.D., Baselga, E., and Graupera, M. (2019). PIK3CA mutations in vascular malformations. Curr Opin
16 Hematol *26*, 170-178.
17 Castillo, S.D., Tzouanacou, E., Zaw-Thin, M., Berenjeno, I.M., Parker, V.E., Chivite, I., Mila-Guasch, M., Pearce,
18 W., Solomon, I., Angulo-Urarte, A., *et al.* (2016). Somatic activating mutations in Pik3ca cause sporadic venous
19 malformations in mice and humans. Science translational medicine *8*, 332ra343.
20 Chen, T.T., Luque, A., Lee, S., Anderson, S.M., Segura, T., and Iruela-Arispe, M.L. (2010). Anchorage of VEGF to
21 the extracellular matrix conveys differential signaling responses to endothelial cells. J Cell Biol *188*, 595-609.
22 Cheng, S.Y., Nagane, M., Huang, H.S., and Cavenee, W.K. (1997). Intracerebral tumor-associated hemorrhage
23 caused by overexpression of the vascular endothelial growth factor isoforms VEGF121 and VEGF165 but not
24 VEGF189. Proc Natl Acad Sci U S A *94*, 12081-12087.
25 Childs, S., Chen, J.N., Garrity, D.M., and Fishman, M.C. (2002). Patterning of angiogenesis in the zebrafish
26 embryo. Development *129*, 973-982.
27 Chung, J., Grammer, T.C., Lemon, K.P., Kazlauskas, A., and Blenis, J. (1994). PDGF- and insulin-dependent
28 pp70S6k activation mediated by phosphatidylinositol-3-OH kinase. Nature *370*, 71-75.
29 Claesson-Welsh, L. (2016). VEGF receptor signal transduction - A brief update. Vascul Pharmacol *86*, 14-17.
30 Costa, G., Harrington, K.I., Lovegrove, H.E., Page, D.J., Chakravartula, S., Bentley, K., and Herbert, S.P. (2016).
31 Asymmetric division coordinates collective cell migration in angiogenesis. Nature cell biology *18*, 1292-1301.
32 Davies, S.P., Reddy, H., Caivano, M., and Cohen, P. (2000). Specificity and mechanism of action of some
33 commonly used protein kinase inhibitors. Biochem J *351*, 95-105.
34 Dayanir, V., Meyer, R.D., Lashkari, K., and Rahimi, N. (2001). Identification of tyrosine residues in vascular
35 endothelial growth factor receptor-2/FLK-1 involved in activation of phosphatidylinositol 3-kinase and cell
36 proliferation. J Biol Chem *276*, 17686-17692.
37 Dejana, E., Hirschi, K.K., and Simons, M. (2017). The molecular basis of endothelial cell plasticity. Nature
38 communications *8*, 14361.
39 Delcombel, R., Janssen, L., Vassy, R., Gammons, M., Haddad, O., Richard, B., Letourneur, D., Bates, D.,
40 Hendricks, C., Waltenberger, J., *et al.* (2013). New prospects in the roles of the C-terminal domains of VEGF-A and
41 their cooperation for ligand binding, cellular signaling and vessels formation. Angiogenesis *16*, 353-371.
42 Fearnley, G.W., Smith, G.A., Abdul-Zani, I., Yuldasheva, N., Mughal, N.A., Homer-Vanniasinkam, S., Kearney,
43 M.T., Zachary, I.C., Tomlinson, D.C., Harrison, M.A., *et al.* (2016). VEGF-A isoforms program differential
44 VEGFR2 signal transduction, trafficking and proteolysis. Biology open *5*, 571-583.
45 Ferrara, N., Carver-Moore, K., Chen, H., Dowd, M., Lu, L., O'Shea, K.S., Powell-Braxton, L., Hillan, K.J., and
46 Moore, M.W. (1996). Heterozygous embryonic lethality induced by targeted inactivation of the VEGF gene. Nature
47 *380*, 439-442.
48 Fish, J.E., Cantu Gutierrez, M., Dang, L.T., Khyzha, N., Chen, Z., Veitch, S., Cheng, H.S., Khor, M., Antounians,
49 L., Njock, M.S., *et al.* (2017). Dynamic regulation of VEGF-inducible genes by an ERK/ERG/p300 transcriptional
50 network. Development *144*, 2428-2444.
51 Fujita, M., Cha, Y.R., Pham, V.N., Sakurai, A., Roman, B.L., Gutkind, J.S., and Weinstein, B.M. (2011). Assembly
52 and patterning of the vascular network of the vertebrate hindbrain. Development *138*, 1705-1715.
53 Gerber, H.P., McMurtrey, A., Kowalski, J., Yan, M., Keyt, B.A., Dixit, V., and Ferrara, N. (1998). Vascular
54 endothelial growth factor regulates endothelial cell survival through the phosphatidylinositol 3'-kinase/Akt signal
55 transduction pathway. Requirement for Flk-1/KDR activation. J Biol Chem *273*, 30336-30343.

Gimbrone, M.A., Jr., and Garcia-Cardena, G. (2016). Endothelial Cell Dysfunction and the Pathobiology of Atherosclerosis. Circ Res *118*, 620-636.

Gong, B., Liang, D., Chew, T.G., and Ge, R. (2004). Characterization of the zebrafish vascular endothelial growth factor A gene: comparison with vegf-A genes in mammals and Fugu. Biochimica et biophysica acta *1676*, 33-40.

Graupera, M., Guillermet-Guibert, J., Foukas, L.C., Phng, L.K., Cain, R.J., Salpekar, A., Pearce, W., Meek, S., Millan, J., Cutillas, P.R., *et al.* (2008). Angiogenesis selectively requires the p110alpha isoform of PI3K to control endothelial cell migration. Nature *453*, 662-666.

Graupera, M., and Potente, M. (2013). Regulation of angiogenesis by PI3K signaling networks. Exp Cell Res *319*, 1348-1355.

Guo, P., Xu, L., Pan, S., Brekken, R.A., Yang, S.T., Whitaker, G.B., Nagane, M., Thorpe, P.E., Rosenbaum, J.S., Su Huang, H.J., *et al.* (2001). Vascular endothelial growth factor isoforms display distinct activities in promoting tumor angiogenesis at different anatomic sites. Cancer Res *61*, 8569-8577.

Hasan, S.S., Tsaryk, R., Lange, M., Wisniewski, L., Moore, J.C., Lawson, N.D., Wojciechowska, K., Schnittler, H., and Siekmann, A.F. (2017). Endothelial Notch signalling limits angiogenesis via control of artery formation. Nature cell biology *19*, 928-940.

Heffron, T.P., Heald, R.A., Ndubaku, C., Wei, B., Augistin, M., Do, S., Edgar, K., Eigenbrot, C., Friedman, L., Gancia, E., *et al.* (2016). The Rational Design of Selective Benzoxazepin Inhibitors of the alpha-Isoform of Phosphoinositide 3-Kinase Culminating in the Identification of (S)-2-((2-(1-Isopropyl-1H-1,2,4-triazol-5-yl)-5,6-dihydrobenzo[f]imidazo[1,2-d][1,4]oxazepin-9-yl)oxy)propanamide (GDC-0326). J Med Chem *59*, 985-1002.

Herve, M.A., Buteau-Lozano, H., Mourah, S., Calvo, F., and Perrot-Applanat, M. (2005). VEGF189 stimulates endothelial cells proliferation and migration in vitro and up-regulates the expression of Flk-1/KDR mRNA. Exp Cell Res *309*, 24-31.

Hogan, B.M., Bos, F.L., Bussmann, J., Witte, M., Chi, N.C., Duckers, H.J., and Schulte-Merker, S. (2009). ccbe1 is required for embryonic lymphangiogenesis and venous sprouting. Nature Genetics *41*, 396-398.

Hogan, B.M., and Schulte-Merker, S. (2017). How to Plumb a Pisces: Understanding Vascular Development and Disease Using Zebrafish Embryos. Dev Cell *42*, 567-583.

Isogai, S., Lawson, N.D., Torrealday, S., Horiguchi, M., and Weinstein, B.M. (2003). Angiogenic network formation in the developing vertebrate trunk. Development *130*, 5281-5290.

Janetopoulos, C., Borleis, J., Vazquez, F., Iijima, M., and Devreotes, P. (2005). Temporal and spatial regulation of phosphoinositide signaling mediates cytokinesis. Dev Cell *8*, 467-477.

Jin, D., Zhu, D., Fang, Y., Chen, Y., Yu, G., Pan, W., Liu, D., Li, F., and Zhong, T.P. (2017). Vegfa signaling regulates diverse artery/vein formation in vertebrate vasculatures. Journal of genetics and genomics = Yi chuan xue bao *44*, 483-492.

Jin, S.W., Beisl, D., Mitchell, T., Chen, J.N., and Stainier, D.Y.R. (2005). Cellular and molecular analyses of vascular tube and lumen formation in zebrafish. Development *132*, 5199-5209.

Kazemi, M., Carrer, A., Moimas, S., Zandona, L., Bussani, R., Casagranda, B., Palmisano, S., Prelazzi, P., Giacca, M., Zentilin, L., *et al.* (2016). VEGF121 and VEGF165 differentially promote vessel maturation and tumor growth in mice and humans. Cancer Gene Ther *23*, 125-132.

Koch, S., and Claesson-Welsh, L. (2012). Signal transduction by vascular endothelial growth factor receptors. Cold Spring Harbor perspectives in medicine *2*, a006502.

Kochhan, E., and Siekmann, A.F. (2013). Zebrafish as a Model to Study Chemokine Function. In Chemokines: Methods and Protocols, E.A. Cardona, and E.E. Ubogu, eds. (Totowa, NJ: Humana Press), pp. 145-159.

Kreis, N.N., Louwen, F., and Yuan, J. (2019). The Multifaceted p21 (Cip1/Waf1/CDKN1A) in Cell Differentiation, Migration and Cancer Therapy. Cancers (Basel) *11*.

Lawson, N.D., Scheer, N., Pham, V.N., Kim, C.H., Chitnis, A.B., Campos-Ortega, J.A., and Weinstein, B.M. (2001). Notch signaling is required for arterial-venous differentiation during embryonic vascular development. Development *128*, 3675-3683.

Lawson, N.D., Vogel, A.M., and Weinstein, B.M. (2002). sonic hedgehog and vascular endothelial growth factor act upstream of the Notch pathway during arterial endothelial differentiation. Dev Cell *3*, 127-136.

Liang, D., Xu, X., Chin, A.J., Balasubramaniyan, N.V., Teo, M.A., Lam, T.J., Weinberg, E.S., and Ge, R. (1998). Cloning and characterization of vascular endothelial growth factor (VEGF) from zebrafish, Danio rerio. Biochimica et biophysica acta *1397*, 14-20.

Mavria, G., Vercoulen, Y., Yeo, M., Paterson, H., Karasarides, M., Marais, R., Bird, D., and Marshall, C.J. (2006). ERK-MAPK signaling opposes Rho-kinase to promote endothelial cell survival and sprouting during angiogenesis. Cancer Cell *9*, 33-44.

29

1   Meadows, K.N., Bryant, P., and Pumiglia, K. (2001). Vascular endothelial growth factor induction of the angiogenic
2   phenotype requires Ras activation. J Biol Chem *276*, 49289-49298.
3   Mitchell, P., Liew, G., Gopinath, B., and Wong, T.Y. (2018). Age-related macular degeneration. Lancet *392*, 1147-
4   1159.
5   Nakatsu, M.N., Sainson, R.C., Perez-del-Pulgar, S., Aoto, J.N., Aitkenhead, M., Taylor, K.L., Carpenter, P.M., and
6   Hughes, C.C. (2003). VEGF(121) and VEGF(165) regulate blood vessel diameter through vascular endothelial
7   growth factor receptor 2 in an in vitro angiogenesis model. Lab Invest *83*, 1873-1885.
8   Nicoli, S., Knyphausen, C.P., Zhu, L.J., Lakshmanan, A., and Lawson, N.D. (2012). miR-221 is required for
9   endothelial tip cell behaviors during vascular development. Dev Cell *22*, 418-429.
10   Ola, R., Dubrac, A., Han, J., Zhang, F., Fang, J.S., Larrivee, B., Lee, M., Urarte, A.A., Kraehling, J.R., Genet, G.*, et*
11   *al.* (2016). PI3 kinase inhibition improves vascular malformations in mouse models of hereditary haemorrhagic
12   telangiectasia. Nature communications *7*, 13650.
13   Overton, K.W., Spencer, S.L., Noderer, W.L., Meyer, T., and Wang, C.L. (2014). Basal p21 controls population
14   heterogeneity in cycling and quiescent cell cycle states. Proc Natl Acad Sci U S A *111*, E4386-4393.
15   Pack, L.R., Daigh, L.H., and Meyer, T. (2019). Putting the brakes on the cell cycle: mechanisms of cellular growth
16   arrest. Curr Opin Cell Biol *60*, 106-113.
17   Pages, G., Guerin, S., Grall, D., Bonino, F., Smith, A., Anjuere, F., Auberger, P., and Pouyssegur, J. (1999).
18   Defective thymocyte maturation in p44 MAP kinase (Erk 1) knockout mice. Science *286*, 1374-1377.
19   Park, J.E., Keller, G.A., and Ferrara, N. (1993). The vascular endothelial growth factor (VEGF) isoforms:
20   differential deposition into the subepithelial extracellular matrix and bioactivity of extracellular matrix-bound
21   VEGF. Mol Biol Cell *4*, 1317-1326.
22   Peach, C.J., Mignone, V.W., Arruda, M.A., Alcobia, D.C., Hill, S.J., Kilpatrick, L.E., and Woolard, J. (2018).
23   Molecular Pharmacology of VEGF-A Isoforms: Binding and Signalling at VEGFR2. Int J Mol Sci *19*.
24   Pontes-Quero, S., Fernandez-Chacon, M., Luo, W., Lunella, F.F., Casquero-Garcia, V., Garcia-Gonzalez, I.,
25   Hermoso, A., Rocha, S.F., Bansal, M., and Benedito, R. (2019). High mitogenic stimulation arrests angiogenesis.
26   Nature communications *10*, 2016.
27   Potente, M., Gerhardt, H., and Carmeliet, P. (2011). Basic and therapeutic aspects of angiogenesis. Cell *146*, 873-
28   887.
29   Qian, X., Hulit, J., Suyama, K., Eugenin, E.A., Belbin, T.J., Loudig, O., Smirnova, T., Zhou, Z.N., Segall, J.,
30   Locker, J.*, et al.* (2013). p21CIP1 mediates reciprocal switching between proliferation and invasion during
31   metastasis. Oncogene *32*, 2292-2303 e2297.
32   Ricard, N., Scott, R.P., Booth, C.J., Velazquez, H., Cilfone, N.A., Baylon, J.L., Gulcher, J.R., Quaggin, S.E.,
33   Chittenden, T.W., and Simons, M. (2019). Endothelial ERK1/2 signaling maintains integrity of the quiescent
34   endothelium. J Exp Med *216*, 1874-1890.
35   Roman, B.L., Pham, V.N., Lawson, N.D., Kulik, M., Childs, S., Lekven, A.C., Garrity, D.M., Moon, R.T., Fishman,
36   M.C., Lechleider, R.J.*, et al.* (2002). Disruption of acvrl1 increases endothelial cell number in zebrafish cranial
37   vessels. Development *129*, 3009-3019.
38   Rossi, A., Gauvrit, S., Marass, M., Pan, L., Moens, C.B., and Stainier, D.Y.R. (2016). Regulation of Vegf signaling
39   by natural and synthetic ligands. Blood *128*, 2359-2366.
40   Ruhrberg, C., Gerhardt, H., Golding, M., Watson, R., Ioannidou, S., Fujisawa, H., Betsholtz, C., and Shima, D.T.
41   (2002). Spatially restricted patterning cues provided by heparin-binding VEGF-A control blood vessel branching
42   morphogenesis. Genes Dev *16*, 2684-2698.
43   Schuermann, A., Helker, C.S., and Herzog, W. (2014). Angiogenesis in zebrafish. Semin Cell Dev Biol *31*, 106-114.
44   Shin, M., Beane, T.J., Quillien, A., Male, I., Zhu, L.J., and Lawson, N.D. (2016). Vegfa signals through ERK to
45   promote angiogenesis, but not artery differentiation. Development *143*, 3796-3805.
46   Shiying, W., Boyun, S., Jianye, Y., Wanjun, Z., Ping, T., Jiang, L., and Hongyi, H. (2017). The Different Effects of
47   VEGFA121 and VEGFA165 on Regulating Angiogenesis Depend on Phosphorylation Sites of VEGFR2. Inflamm
48   Bowel Dis *23*, 603-616.
49   Sidi, S., Sanda, T., Kennedy, R.D., Hagen, A.T., Jette, C.A., Hoffmans, R., Pascual, J., Imamura, S., Kishi, S.,
50   Amatruda, J.F.*, et al.* (2008). Chk1 suppresses a caspase-2 apoptotic response to DNA damage that bypasses p53,
51   Bcl-2, and caspase-3. Cell *133*, 864-877.
52   Siekmann, A.F., and Lawson, N.D. (2007). Notch signalling limits angiogenic cell behaviour in developing
53   zebrafish arteries. Nature *445*, 781-784.
54   Siekmann, A.F., Standley, C., Fogarty, K.E., Wolfe, S.A., and Lawson, N.D. (2009). Chemokine signaling guides
55   regional patterning of the first embryonic artery. Gene Dev *23*, 2272-2277.
56   Simons, M., and Eichmann, A. (2015). Molecular controls of arterial morphogenesis. Circ Res *116*, 1712-1724.

1 Simons, M., Gordon, E., and Claesson-Welsh, L. (2016). Mechanisms and regulation of endothelial VEGF receptor
2 signalling. Nat Rev Mol Cell Biol *17*, 611-625.
3 Spencer, S.L., Cappell, S.D., Tsai, F.C., Overton, K.W., Wang, C.L., and Meyer, T. (2013). The proliferation-
4 quiescence decision is controlled by a bifurcation in CDK2 activity at mitotic exit. Cell *155*, 369-383.
5 Srinivasan, R., Zabuawala, T., Huang, H., Zhang, J., Gulati, P., Fernandez, S., Karlo, J.C., Landreth, G.E., Leone,
6 G., and Ostrowski, M.C. (2009). Erk1 and Erk2 regulate endothelial cell proliferation and migration during mouse
7 embryonic angiogenesis. PLoS One *4*, e8283.
8 Stalmans, I., Ng, Y.S., Rohan, R., Fruttiger, M., Bouche, A., Yuce, A., Fujisawa, H., Hermans, B., Shani, M.,
9 Jansen, S.*, et al.* (2002). Arteriolar and venular patterning in retinas of mice selectively expressing VEGF isoforms.
10 J Clin Invest *109*, 327-336.
11 Sugden, W.W., Meissner, R., Aegerter-Wilmsen, T., Tsaryk, R., Leonard, E.V., Bussmann, J., Hamm, M.J., Herzog,
12 W., Jin, Y., Jakobsson, L.*, et al.* (2017). Endoglin controls blood vessel diameter through endothelial cell shape
13 changes in response to haemodynamic cues. Nature cell biology *19*, 653-665.
14 Takahashi, T., Ueno, H., and Shibuya, M. (1999). VEGF activates protein kinase C-dependent, but Ras-independent
15 Raf-MEK-MAP kinase pathway for DNA synthesis in primary endothelial cells. Oncogene *18*, 2221-2230.
16 Tanaka, H., Yamashita, T., Asada, M., Mizutani, S., Yoshikawa, H., and Tohyama, M. (2002). Cytoplasmic
17 p21(Cip1/WAF1) regulates neurite remodeling by inhibiting Rho-kinase activity. J Cell Biol *158*, 321-329.
18 Taylor, J.S., Braasch, I., Frickey, T., Meyer, A., and Van de Peer, Y. (2003). Genome duplication, a trait shared by
19 22000 species of ray-finned fish. Genome research *13*, 382-390.
20 Taylor, J.S., Van de Peer, Y., Braasch, I., and Meyer, A. (2001). Comparative genomics provides evidence for an
21 ancient genome duplication event in fish. Philos Trans R Soc Lond B Biol Sci *356*, 1661-1679.
22 Testini, C., Smith, R.O., Jin, Y., Martinsson, P., Sun, Y., Hedlund, M., Sainz-Jaspeado, M., Shibuya, M., Hellstrom,
23 M., and Claesson-Welsh, L. (2019). Myc-dependent endothelial proliferation is controlled by phosphotyrosine 1212
24 in VEGF receptor-2. EMBO Rep *20*, e47845.
25 Thisse, C., and Thisse, B. (2008). High-resolution in situ hybridization to whole-mount zebrafish embryos. Nat
26 Protoc *3*, 59-69.
27 Ulrich, F., Ma, L.H., Baker, R.G., and Torres-Vazquez, J. (2011). Neurovascular development in the embryonic
28 zebrafish hindbrain. Dev Biol *357*, 134-151.
29 Vempati, P., Popel, A.S., and Mac Gabhann, F. (2014). Extracellular regulation of VEGF: isoforms, proteolysis, and
30 vascular patterning. Cytokine Growth Factor Rev *25*, 1-19.
31 Viallard, C., and Larrivee, B. (2017). Tumor angiogenesis and vascular normalization: alternative therapeutic
32 targets. Angiogenesis *20*, 409-426.
33 Villefranc, J.A., Amigo, J., and Lawson, N.D. (2007). Gateway compatible vectors for analysis of gene function in
34 the zebrafish. Dev Dyn *236*, 3077-3087.
35 Vlahos, C.J., Matter, W.F., Hui, K.Y., and Brown, R.F. (1994). A specific inhibitor of phosphatidylinositol 3-kinase,
36 2-(4-morpholinyl)-8-phenyl-4H-1-benzopyran-4-one (LY294002). J Biol Chem *269*, 5241-5248.
37 Westerfield, M. (1993). The zebrafish book : a guide for the laboratory use of zebrafish (Brachydanio rerio)
38 (Eugene, OR: M. Westerfield).
39 Wong, T.Y., Cheung, C.M., Larsen, M., Sharma, S., and Simo, R. (2016). Diabetic retinopathy. Nat Rev Dis Primers
40 *2*, 16012.
41 Woolard, J., Bevan, H.S., Harper, S.J., and Bates, D.O. (2009). Molecular diversity of VEGF-A as a regulator of its
42 biological activity. Microcirculation *16*, 572-592.
43 Workman, P., Clarke, P.A., Raynaud, F.I., and van Montfort, R.L. (2010). Drugging the PI3 kinome: from chemical
44 tools to drugs in the clinic. Cancer Res *70*, 2146-2157.
45 Zhou, B.P., Liao, Y., Xia, W., Spohn, B., Lee, M.H., and Hung, M.C. (2001). Cytoplasmic localization of
46 p21Cip1/WAF1 by Akt-induced phosphorylation in HER-2/neu-overexpressing cells. Nature cell biology *3*, 245-
47 252.
48
49
50
51

1 **FIGURE LEGENDS**

2 **Figure 1. Mutations in vegfaa and vegfab affect hindbrain blood vessel formation**

3 (A-B) Schematic presentation of zinc finger nuclease or TALEN target site at the

4 genomic sequence for *vegfaa* (A) and *vegfab* (B). Black boxes in the gene structure

5 represent exons and dashed lines represent introns, yellow triangle indicates the

6 position of the targeting sites. Protein domains are displayed below in comparison with

7 wild type protein. Black boxes represent sequences that are not annotated, red boxes

8 are cystine-knot cytokine domains and yellow boxes are heparin binding domains.

9 (C) Cartoon of 58 hpf embryo, arrow indicates imaged region. (D-N) Maximum intensity

10 projection of confocal z-stacks of *Tg(kdrl:EGFP)$_{s843}$* wild type (D), *vegfaa$_{mu128}$* (G),

11 *vegfab$_{mu155}$* (J) and double mutant (M) embryos. Smaller rectangular panels (E, H, K

12 and N) show cropped ventral region of the maximum intensity projection for better

13 visualization of the basilar artery (BA). Dorsal views, anterior to the left. Scale bar = 100

14 um.

15 (F, I, L, O) Graphical representation of hindbrain vascular phenotypes, indicating the

16 position of Primordial hindbrain channel (PHBC)-Central artery (CtA) connections (red

17 filled circles), CtA-CtA connections (black dots) and CtA-BA-Posterior Communicating

18 segments (PCS) connections (yellow filled circles).

19 (P) Quantification of CtA number in wild type (n = 10), *vegfaa$_{mu128}$* (n = 10), *vegfab$_{mu155}$*

20 (n = 10) and double mutant embryos (n = 10). Values are mean±s.d.; n.s = not

21 significant; **** p<0.0001.

1   (Q-S) Maximum intensity projections of confocal z-stacks of *Tg(kdrl:Hsa.HRAS-*

2   *mCherry)$_{s916}$; (fli1a:nEGFP)$_{y7}$* wt (Q), *vegfaa$_{mu128}$* (R) and *vegfab$_{mu155}$* embryos (S).

3   Dorsal view, anterior to the left. Scale bar = 100 um.

4   (T-X) Quantification of the total cell numbers (T) as well as in the PHBC (U), BA (V)

5   CtAs (W) and cells per CtA (X), for wt embryos (n = 6) compared to *vegfaa$_{mu128}$* (n = 6)

6   and *vegfab$_{mu155}$* (n = 5) mutants. Dots represent individual embryos; black lines indicate

7   the mean value±s.d.; n.s = not significant; ** p>0.0022; *** p>0.0003; **** p<0.0001.

8

9   **Figure 2. Analysis of endothelial cell migration and proliferation in the trunk**

10   **vasculature of *vegfaa$_{mu128}$* and *vegfab$_{mu155}$* mutants**

11   (A-F) Maximum intensity projections of confocal z-stacks of *Tg(kdrl:Hsa.HRAS-*

12   *mCherry)$_{s916}$; (fli1a:nEGFP)$_{y7}$* wt (A-B), heterozygous *vegfaa$_{mu128}$* (C-D) and *vegfab$_{mu155}$*

13   (E-F) embryos; lateral view, anterior to the left. Scale bar = 100 um.

14   (G) Quantification of endothelial cell numbers per intersegmental blood vessel sprout

15   (ISV) in wt (n = 12), heterozygous *vegfaa$_{mu128}$* (n = 26) and *vegfab$_{mu155}$* (n = 14) mutants

16   at 32 hpf. Dots represent individual embryos; black lines indicate the mean value ±s.d.;

17   **** p<0.0001.

18   (H-K) Confocal time-lapse images of individual sprouting ISV showing tip cell migration

19   (arrowheads) in wt (H), heterozygous *vegfaa$_{mu128}$* (I), severely affected heterozygous

20   *vegfaa$_{mu128}$* (J) and homozygous *vegfab$_{mu155}$* (K) embryos; lateral view, anterior to the

21   left. Scale bar = 20 um.

22   (L) Quantification of tip cell migration, measuring the dorsal movement of cell nuclei for

23   wild type (grey; n = 13 ISVs, 4 embryos), *vegfaa$_{mu128+/-}$* (blue; n = 11 ISVs, 4 embryos),

1   *vegfaa$_{mu128\ +/-}$* severe (yellow; n = 11 ISVs, 4 embryos) and *vegfab$_{mu155\ -/-}$* (red; n = 11

2   ISVs, 4 embryos). Values are mean±s.d.

3   (M-O) Confocal time-lapse images of 10 growing ISVs in wild type (M), *vegfaa$_{mu128+/-}$* (N)

4   and *vegfab$_{mu155\ -/-}$* (O) embryos (n=4 each) that were analyzed for cell proliferation.

5   Arrowheads indicate cells derived from proliferation. Lateral views, anterior to the left.

6   Scale bar = 100 um.

7   (P) Quantification of proliferation events per ISV during 10 h of time lapse imaging from

8   22 - 32 hpf in wild type (n = 40 ISVs, 4 embryos), *vegfaa$_{mu128+/-}$* (n = 40 ISVs, 4

9   embryos) and *vegfab$_{mu155\ -/-}$* (n = 50 ISVs, 5 embryos). Dots represent individual

10   embryos; black lines indicate the mean value ±s.d.; ** p>0.0022.

11

12   **Figure 3. Vegfab is not essential for ERK phosphorylation or *dll4* and *flt4***

13   **expression in sprouting ISVs**

14   (A-B) High magnification of confocal z-stack of anti-pERK antibody staining on

15   transgenic *Tg(fli:nEGFP)$_{y7}$* embryos with quantitative heat map of pERK staining at 28

16   hpf for wt (A) and *vegfab$_{mu155}$* (B) embryos, lateral view, anterior to the left. Scale bar =

17   20 um.

18   (C) Quantification of pERK staining intensity of every ISV cell represented in relative

19   units (R.U.) for wt (n = 5) and v*egfab$_{mu155}$* (n = 8) at 28 hpf. Dots represent individual

20   embryos; black lines indicate the mean value±s.d. n.s = not significant.

21   (D-K) Whole mount in situ hybridization for dll4 (D-G) and flt4 (H-K) on wt (D-E and H-I))

22   and *vegfab$_{mu155}$* (F-G and J-K) embryos at 23 or 28 hpf. Lateral views, anterior to the

23   left. Scale bar = 100 um.

34

1   (L-Q) Maximum intensity projections of *Tg(kdrl:HsaHRAS-mCherry)s916*; *(fli1a:nEGFP)y7*

2   embryos treated with DMSO (L-N; n=13) or with 0.25 um PMA (O-Q; n=10).

3   (R-W) Maximum intensity projections of *Tg(kdrl:HsaHRASmCherry)s916*; *(fli1a:nEGFP)y7*

4   v*egfabmu155* mutant embryos treated with DMSO (R-T; n=11) or v*egfabmu155* mutant

5   embryos treated with PMA (U-W; n=10). Lateral views, anterior to the left. Scale bar =

6   100 um.

7   (X) Quantification of endothelial cell numbers. Dots represent individual embryos; black

8   lines indicate the mean value±s.d.; **** p<0.0001. Scale bar=100 um.

9

10   **Figure 4. LY294002 mediated inhibition of PI3K affects endothelial cell**

11   **proliferation**

12   (A-F) Maximum intensity projection of a confocal z-stack of the trunk vasculature of

13   double transgenic *Tg(kdrl:Hsa.HRAS-mCherry)s916*; *(fli1a:nEGFP)y7* wt embryos treated

14   with DMSO (A-C) or 10 uM LY294002 (D-F) at 32 hpf. Lateral views, anterior to the left.

15   Scale bar = 100 um.

16   (G) Quantification of the cells per ISV in DMSO treated embryos (n = 24) compared to

17   LY294002 treated embryos(n = 25). Dots represent individual embryos; black lines

18   indicate the mean value ±s.d. **** p<0.0001.

19   (H, I) Confocal time-lapse images of individual sprouting ISV showing tip cell migration

20   (arrowheads) in wt embryos treated with DMSO (H) or LY294002 (I) starting from 22

21   hpf for 6 h. Scale bar = 20 um.

1   (J) Quantification of tip cell migration, measuring the dorsal movement of cell nuclei for

2   wild type embryos treated with DMSO (grey; 11 ISVs,3 embryos) or LY294002 (blue; 11

3   ISVs, 4 embryos); Values are mean±s.d.

4   (K, L) Confocal time-lapse images of 10 growing ISVs in embryos treated with DMSO

5   (K) or with LY294002 (L) that were analyzed for cell proliferation. Arrowheads indicate

6   cells derived from proliferation. Scale bar = 100 um.

7   (M) Quantification of proliferation events in ISVs during 10 h of time lapse imaging from

8   22 - 32 hpf after DMSO (n = 30 ISVs, 3 embryos) or LY294002 (n = 40 ISVs, 4

9   embryos) treatment. Dots represent individual embryos; black lines indicate the mean

10   value±s.d.; ** p>0.0022.

11

12   **Figure 5. Vegfab / PI3K signaling influences Cdkn1a/p21 expression and**

13   **localization**

14   (A) Cartoon depicting experimental set up for FACS and qPCR experiment. Triple

15   transgenic embryos *Tg(kdrl:Hsa.HRAS-mCherry)s916; (dll4:gal4)mu106; (UAS:gfp)nkuasgfp1a*

16   were injected with vegfab or control morpholino at the 1 cell stage and raised to 28 hpf.

17   Embryos were dissociated and GFP/mCherry positive cells were FACS sorted.

18   (B) Expression of cell cycle regulators cdk2, cdkn1a/p21 and cdkn1b/p27 comparing

19   cells from vegfab morpholino injected embryos with control morpholino injected

20   embryos, which were set as 1 (n = 3 independent experiments). Expression data are

21   shown as fold change; dots represent individual experiments; black lines indicate the

22   mean value±s.d.; ** p>0.0022.

36

1 (C) Western Blot of proteins from Human Umbilical Vein Endothelial Cells showing

2 decrease in AKT phosphorylation, while no change in Cdkn1a/p21 protein amount

3 following LY294002 treatment was detected. Representative blot of n=3 is shown.

4 (D-I) Confocal images of Human Umbilical Vein Endothelial Cells treated with DMSO

5 (D-F) or LY294002 (G-I). HOECHST staining labels nuclei, Cdkn1a/p21 protein in red,

6 scale bar is 200 um.

7 (J) Quantification of nuclear fluorescence of Cdkn1a/p21 protein in DMSO (n=6

8 experiments) or LY294002 (n=6 experiments) treated Human Umbilical Vein Endothelial

9 Cells in relative units (R.U.). Dots represent individual experiments; black lines indicate

10 the mean value±s.d.; ** p>0.0022.

11

12 **Figure 6. Cdkn1a/p21 knock down in zebrafish embryos rescues proliferation**

13 **defects resulting from *vegfab* deficiency or PI3K inhibition**

14 (A-D) Maximum intensity projection of a confocal z-stack of the trunk vasculature of

15 double transgenic *Tg(kdrl:Hsa.HRAS-mCherry)$_{s916}$*; *Tg(fli1a:nEGFP)$_{y7}$* wild type

16 embryos (A-B) or *vegfab$_{mu155}$* embryos (C-D) at 32 hpf, injected with either control

17 morpholino (A, C) or Cdkn1a/p21 morpholino (B, D). Lateral view; anterior to the left.

18 Scale bars = 100 um.

19 (E) Quantification of cells per ISV in wt (n=12) and *vegfab$_{mu155}$* (n=10) embryos injected

20 with control or Cdkn1a/p21 morpholino (MO). Dots represent individual embryos; black

21 lines indicate the mean value ±s.d. n.s = not significant; * p>0.05; *** p>0.0003; ****

22 p<0.0001.

1   (F-I) Maximum intensity projection of a confocal z-stack of the trunk vasculature of 32

2   hpf double transgenic *Tg(kdrl:Hsa.HRAS-mCherry)*$_{s916}$; *Tg(fli1a:nEGFP)*$_{y7}$ embryos

3   injected with ctr. morpholino (F, H) or cdkn1a/p21 morpholino (G, I) that were also

4   treated with either DMSO (F-G) or 10 uM LY294002 (H-I). Lateral view; anterior to the

5   left. Scale bars = 100 um.

6   (J) Quantification of cells per ISV at 32 hpf for Ctr. MO + DMSO, Ctr. morpholino +

7   LY294002, cdkn1a/p21 MO + DMSO and cdkn1a/p21 MO + LY294002 (n = 21 embryos

8   in each group); black lines indicate the mean value ±s.d. n.s = not significant; * p>0.05;

9   *** p>0.0003; **** p<0.0001.

10

11 **Figure 7. Inhibiting PI3 kinase signaling during retinal angiogenesis reduces**

12 **endothelial cell proliferation**

13 (A) Representative confocal micrograph of a vehicle treated P6 retina. Endothelial cell

14 nuclei are labelled in red by ERG, EdU incorporation in blue and overlay of red and blue

15 channels is pseudocolored in green. Boxed area is magnified in (C).

16 (B) Representative confocal micrograph of a GDC-0941 treated P6 retina. Boxed area is

17 magnified in (D). Scale bar is 150 um.

18 (C) Magnified image of angiogenic front in vehicle treated retina.

19 (D) Magnified image of GDC-0941 treated retina.

20 (E) Magnified image of vehicle treated vein.

21 (F) Magnified image of GDC-0941 treated vein.

1   (G) Quantification of percentage of EdU positive ERG positive cells in vehicle or GDC-

2   0941 treated retinas at the angiogenic front. Each dot represents a retina flank. For

3   vehicle treated group n=4 (7 retinas), for GDC-0941 treated group n=5 (10 retinas).

4   (H) Quantification of percentage of EdU positive ERG positive cells in vehicle or GDC-

5   0941 treated retinas in the vein area. Each dot represents a retina flank. For vehicle

6   treated group n=4 (7 retinas), for GDC-0941 treated group n=5 (10 retinas).

7

8   **Supplementary Figure S1. Distinct sprouting and proliferation defects in *vegfaa***

9   **or *vegfab* mutants correlate with *vegfaa* and *vegfab* expression domains**

10   (A-D) Fluorescent in situ hybridization combined with an anti-EGFP antibody staining

11   showing the distribution of vegfaa121 (red, A-B), vegfab171 (red, C-D) and EGFP

12   driven by *Tg(Kdrl:EGFP)$_{s843}$* (green, B, D) at 32 hpf. Dorsal views anterior to the left.

13   Arrows indicate the expression domains of vegfaa and vegfab. Scale bar = 100 um.

14   (E-G) Still images of confocal time-lapse of zebrafish hindbrain development in live

15   *Tg(kdrl:Hsa.HRAS-mCherry)$_{s916}$*; *Tg(fli1a:nEGFP)$_{y7}$* embryos between 32 and 42 hpf,

16   shown for wild type (E), vegfaa$_{mu128}$ (F) and vegfab$_{mu155}$ (G). Dorsal view, anterior to the

17   left, Scale bar = 100 um. White dots mark cells within CtAs derived from proliferation.

18   (H) Quantification of cell numbers derived from proliferation and total cell numbers in

19   wild type, *vegfaa$_{mu128}$* and *vegfab$_{mu155}$* embryos (n = 3 embryos for each group). Dots

20   represent individual embryos; black lines indicate the mean value±s.d. n.s. = not

21   significant; * $p > 0.05$; ** $p > 0.0022$; **** $p < 0.0001$.

22   (I) Quantification of cells derived from proliferation normalized to the total cell number

23   comparing wild type, *vegfaa$_{mu128}$* and *vegfab$_{mu155}$* (n = 3 embryos for each group). Dots

1   represent individual embryos; black lines indicate the mean value±s.d. n.s = not

2   significant; ** p>0.0022.

3

4   **Supplementary Figure S2. Analysis of overall morphology and ISV formation in**

5   **vegfaa_{mu128} and vegfab_{mu155} mutants at 30 hpf**

6   (A, C, E, G and I) Brightfield images of wild type (A), *vegfaa_{mu128 +/-}* (C), *vegfaa_{mu128 -/-}*

7   (E) *vegfab_{mu155 +/-}* (G) and *vegfab_{mu155 -/-}* (I) embryos. (B, D, F, H and J) Maximum

8   intensity projections of confocal z-stacks of the trunk vasculature of *Tg(kdrl:EGFP)_{s843}*

9   wild type (B), *vegfaa_{mu128 +/-}* (D), *vegfaa_{mu128 -/-}* (F) *vegfab_{mu155 +/-}* (H) and *vegfab_{mu155 -/-}*

10   (J) embryos. Lateral views, anterior to the left. Scale bar = 100 um.

11   (K) Quantification of ISV length from ISV number 1 to number 10 from anterior to

12   posterior of the trunk vasculature of wild type (green), *vegfaa_{mu128 +/-}* (red), *vegfaa_{mu128 -/-}*

13   (black) *vegfab_{mu155 +/-}* (brown) and *vegfab_{mu155 -/-}* (blue) embryos; n = 8. Values are

14   mean±s.d.

15

16   **Supplementary Figure S3. Overexpression of Vegfab leads to an increase in ISV**

17   **cell numbers**

18   (A-C) ISVs of uninjected control embryos at 32 hpf. Blood vessels labelled by

19   *Tg(Hsa.HRAS-mCherry)_{s916}* in red (A). Endothelial cell nuclei labelled by

20   *Tg(Fli:nEGFP)_{y7}* in green (B). Overlay of red and green channels (C). Side views,

21   anterior to the left.

22   (D-F) ISVs of embryos injected with 50pg of vegfab mRNA at 32 hpf. Blood vessels

23   labelled by *Tg(Hsa.HRAS-mCherry)_{s916}* in red (D). Endothelial cell nuclei labelled by

1   *Tg(Fli:nEGFP)y7* in green (E). Overlay of red and green channels (F). Scale bar is 50

2   um.

3   (G) Quantification of ISV cell numbers in control and vegfab mRNA injected embryos

4   (n=17 embryos each).

5

6   **Supplementary Figure S4. PMA treatment of zebrafish embryos leads to ERK**

7   **phosphorylation**

8   (A-B) Overview pictures of wild type embryos at 32 hpf treated with DMSO (A) or 0.25

9   uM PMA (B). Scale bar = 400 um.

10   (C) Western blot analysis of pERK, total ERK and Actin in embryos treated with

11   indicated concentrations of PMA or DMSO. Representative western blot of n=3 is

12   shown.

13

14   **Supplementary Figure S5. LY294002 treatment of zebrafish embryos leads to a**

15   **reduction in Akt phosphorylation**

16   (A-B) Brightfield images of single wild type embryos at 32 hpf treated with DMSO (A) or

17   10 uM LY294002 (B). Lateral views, anterior to the left. Scale bar = 400 um.

18   (C) Western blot analysis of pAKT, total AKT and Actin in embryos treated with DMSO

19   or 10 uM LY294002. Representative blot of n=3 is shown.

20

21

22

1 **Supplementary Figure S6. GDC-0326 mediated inhibition of PI3K p110 alpha**

2 **isoform affects endothelial cell numbers**

3 (A) Western blot analysis of pAKT, total AKT and Actin in embryos treated with DMSO

4 or indicated concentrations of GDC-0326. Representative blot of n=3 is shown.

5 (B-M) Maximum intensity projection of confocal z-stacks of the trunk vasculature of

6 double transgenic *Tg(kdrl:Hsa.HRAS-mCherry)$_{s916}$*; *Tg(fli1a:nEGFP)$_{y7}$* embryos treated

7 with DMSO (B-D), 10 uM GDC-0326 (E-G), 25 uM GDC-0326 (H-J) or 50 uM GDC-

8 0326 (K-M). Lateral views, anterior to the left. Scale bar = 100 um.

9 (N) Quantification of cells per ISV in embryos treated with DMSO compared to embryos

10 treated with 10 uM, 25 uM and 50 uM GDC-0326. Dots represent individual embryos (n

11 = 14 embryos for each condition), black lines indicate the mean value ±s.d. ***

12 p>0.0003; **** p<0.0001.

13

14 **Supplementary Figure S7. Treatment of mouse retinas with GDC-0941 leads to**

15 **reduction in AKT phosphorylation and S6 phosphorylation**

16 (A) Western blot analysis of pAKT, total AKT and CD144/Cdh5. Representative blot of

17 n=3 is shown.

18 (B-C) Immunohistochemistry on mouse retina. Staining for isolectinB4 (blue; blood

19 vessels) and pS6 kinase (red) in vehicle injected control mice (B, C) and GDC-0941

20 injectected mice (D, E). Scale bar is 150 um.

21

22

42

Supplementary Video S1. Development of hindbrain vasculature in wildtype zebrafish embryo

Endothelial cells are marked by virtue of EGFP expression in $Tg(kdrl:EGFP)_{s843}$ zebrafish. Dorsal view of head region, anterior to the left. Imaging starts at 28 hpf and is carried out for 18.5 hours.

Supplementary Video S2. Development of hindbrain vasculature in $vegfaa_{mu128}$ zebrafish embryo

Endothelial cells are marked by virtue of EGFP expression in $Tg(kdrl:EGFP)_{s843}$ zebrafish. Dorsal view of head region, anterior to the left. Imaging starts at 28 hpf and is carried out for 18.5 hours.

Supplementary Video S3. Development of hindbrain vasculature in $vegfab_{mu155}$ zebrafish embryo

Endothelial cells are marked by virtue of EGFP expression in $Tg(kdrl:EGFP)_{s843}$ zebrafish. Dorsal view of head region, anterior to the left. Imaging starts at 28 hpf and is carried out for 18.5 hours.

Supplementary Video S4. Development of hindbrain vasculature in wildtype zebrafish embryo

Endothelial cell membranes (red) are marked by virtue of mCherry expression, while endothelial cell nuclei express EGFP (green) in $Tg(kdrl:Hsa.HRAS-mCherry)_{s916}$;

1   *Tg(fli1:nEGFP)$_{y7}$* zebrafish. Dorsal view of head region, anterior to the left. Imaging

2   starts at 28 hpf and is carried out for 14 hours.

3

4   **Supplementary Video S5. Development of hindbrain vasculature in *vegfaa$_{mu128}$***

5   **zebrafish embryo**

6   Endothelial cell membranes (red) are marked by virtue of mCherry expression, while

7   endothelial cell nuclei express EGFP (green) in *Tg(kdrl:Hsa.HRAS-mCherry)$_{s916}$*;

8   *Tg(fli1:nEGFP)$_{y7}$* zebrafish. Dorsal view of head region, anterior to the left. Imaging

9   starts at 28 hpf and is carried out for 14 hours.

10

11   **Supplementary Video S6. Development of hindbrain vasculature in *vegfab$_{mu155}$***

12   **zebrafish embryo**

13   Endothelial cell membranes (red) are marked by virtue of mCherry expression, while

14   endothelial cell nuclei express EGFP (green) in *Tg(kdrl:Hsa.HRAS-mCherry)$_{s916}$*;

15   *Tg(fli1:nEGFP)$_{y7}$* zebrafish. Dorsal view of head region, anterior to the left. Imaging

16   starts at 28 hpf and is carried out for 14.5 hours.

17

18   **Supplementary Video S7. Endothelial cell proliferation and migration in individual**

19   **intersegmental blood vessel sprout in wildtype zebrafish embryo**

20   Endothelial cell membranes (red) are marked by virtue of mCherry expression, while

21   endothelial cell nuclei express EGFP (green) in *Tg(kdrl:Hsa.HRAS-mCherry)$_{s916}$*;

22   *Tg(fli1:nEGFP)$_{y7}$* zebrafish. Side view of trunk region, anterior to the left. Imaging starts

1   at 22 hpf and is carried out for 6 hours. Individual endothelial cells are marked by

2   arrowheads and numbers. Decimal numbers indicate progeny after division.

3

4   **Supplementary Video S8. Endothelial cell proliferation and migration in individual**

5   **intersegmental blood vessel sprout in *vegfaamu128* heterozygous zebrafish embryo**

6   Endothelial cell membranes (red) are marked by virtue of mCherry expression, while

7   endothelial cell nuclei express EGFP (green) in *Tg(kdrl:Hsa.HRAS-mCherry)s916*;

8   *Tg(fli1:nEGFP)y7* zebrafish. This example shows intersegmental vessel with normal

9   endothelial cell behaviors. Side view of trunk region, anterior to the left. Imaging starts

10 at 22 hpf and is carried out for 6 hours. Individual endothelial cells are marked by

11 arrowheads and numbers. Decimal numbers indicate progeny after division.

12

13 **Supplementary Video S9. Endothelial cell proliferation and migration in individual**

14 **intersegmental blood vessel sprout in *vegfaamu128* heterozygous zebrafish embryo**

15 Endothelial cell membranes (red) are marked by virtue of mCherry expression, while

16 endothelial cell nuclei express EGFP (green) in *Tg(kdrl:Hsa.HRAS-mCherry)s916*;

17 *Tg(fli1:nEGFP)y7* zebrafish. This example shows a stalled intersegmental vessel. Side

18 view of trunk region, anterior to the left. Imaging starts at 22 hpf and is carried out for 6

19 hours. Individual endothelial cells are marked by arrowheads and numbers. Decimal

20 numbers indicate progeny after division.

21

1 **Supplementary Video S10. Endothelial cell proliferation and migration in**

2 **individual intersegmental blood vessel sprout in *vegfab_{mu155}* mutant zebrafish**

3 **embryo**

4 Endothelial cell membranes (red) are marked by virtue of mCherry expression, while

5 endothelial cell nuclei express EGFP (green) in *Tg(kdrl:Hsa.HRAS-mCherry)_{s916}*;

6 *Tg(fli1:nEGFP)_{y7}* zebrafish Side view of trunk region, anterior to the left. Imaging starts

7 at 22 hpf and is carried out for 6 hours. Individual endothelial cells are marked by

8 arrowheads and numbers. Decimal numbers indicate progeny after division.

9

10 **Supplementary Video S11. Endothelial cell proliferation and migration in**

11 **intersegmental blood vessel sprouts in wildtype zebrafish embryo**

12 Endothelial cell membranes (red) are marked by virtue of mCherry expression, while

13 endothelial cell nuclei express EGFP (green) in *Tg(kdrl:Hsa.HRAS-mCherry)_{s916}*;

14 *Tg(fli1:nEGFP)_{y7}* zebrafish. Side view of trunk region, anterior to the left. Imaging starts

15 at 22 hpf and is carried out for 10 hours. Individual endothelial cells are marked by

16 arrowheads and numbers. Decimal numbers indicate progeny after division.

17

18 **Supplementary Video S12. Endothelial cell proliferation and migration in**

19 **intersegmental blood vessel sprouts in *vegfaa_{mu128}* heterozygous embryo**

20 Endothelial cell membranes (red) are marked by virtue of mCherry expression, while

21 endothelial cell nuclei express EGFP (green) in *Tg(kdrl:Hsa.HRAS-mCherry)_{s916}*;

22 *Tg(fli1:nEGFP)_{y7}* zebrafish. Side view of trunk region, anterior to the left. Imaging starts

1   at 22 hpf and is carried out for 10.5 hours. Individual endothelial cells are marked by

2   arrowheads and numbers. Decimal numbers indicate progeny after division.

3

4   **Supplementary Video S13. Endothelial cell proliferation and migration in**

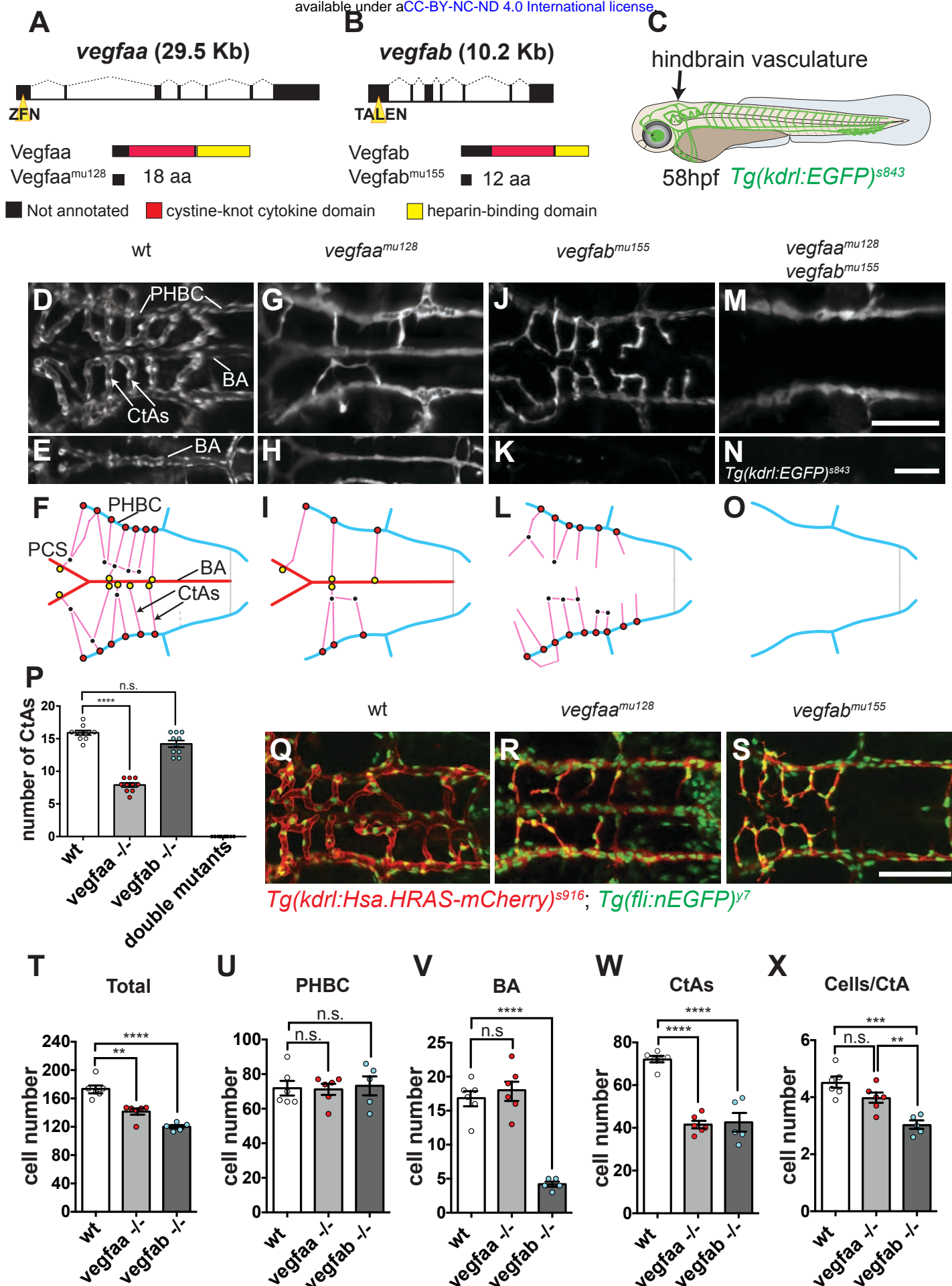5   **intersegmental blood vessel sprouts in *vegfab$_{mu155}$* mutant embryo**

6   Endothelial cell membranes (red) are marked by virtue of mCherry expression, while

7   endothelial cell nuclei express EGFP (green) in *Tg(kdrl:Hsa.HRAS-mCherry)$_{s916}$*;

8   *Tg(fli1:nEGFP)$_{y7}$* zebrafish. Side view of trunk region, anterior to the left. Imaging starts

9   at 22 hpf and is carried out for 10.5 hours. Individual endothelial cells are marked by

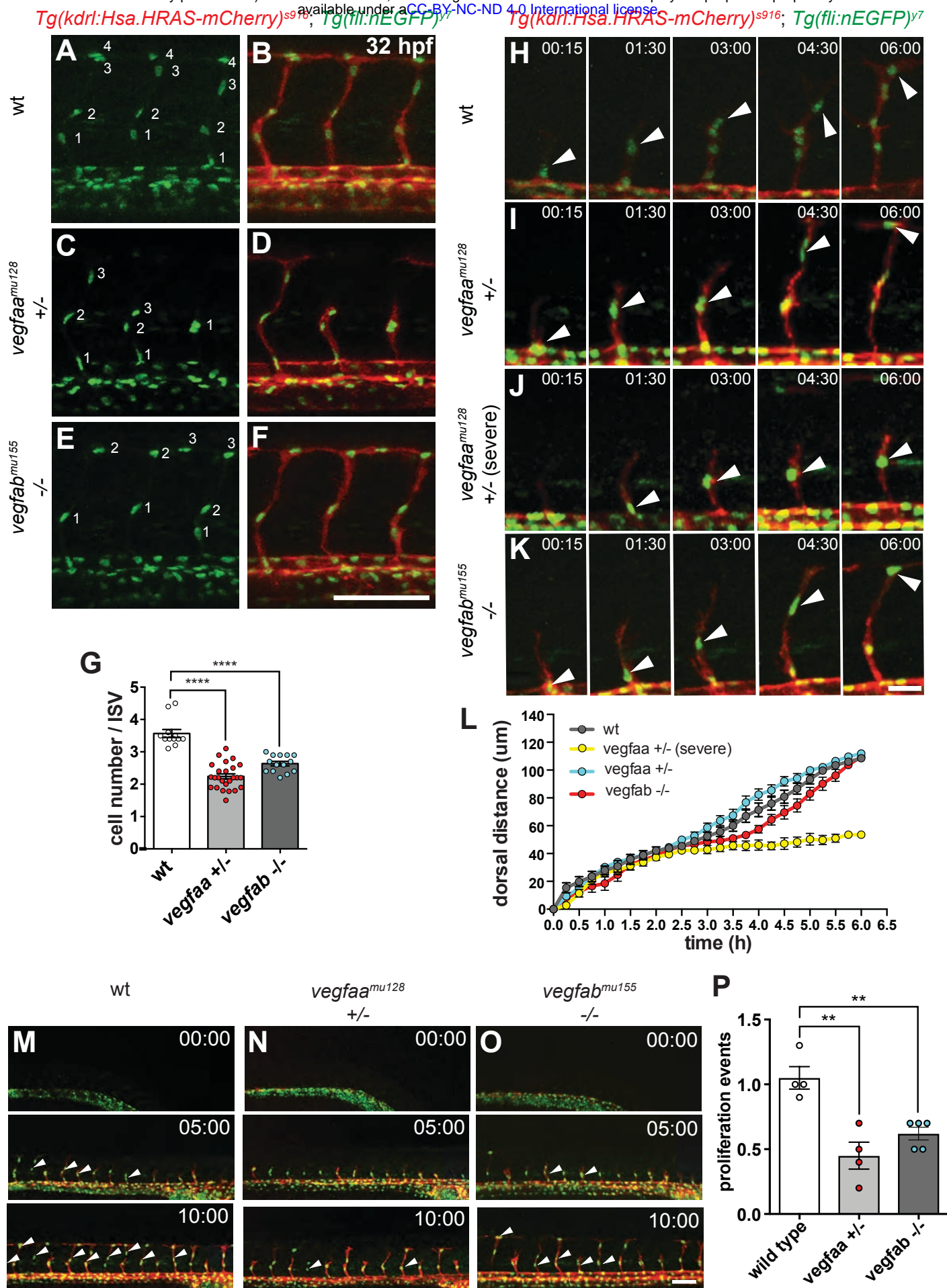10   arrowheads and numbers. Decimal numbers indicate progeny after division.

11

12   **Supplementary Video S14. Endothelial cell proliferation and migration in**

13   **individual intersegmental blood vessel sprout in DMSO treated zebrafish embryo**
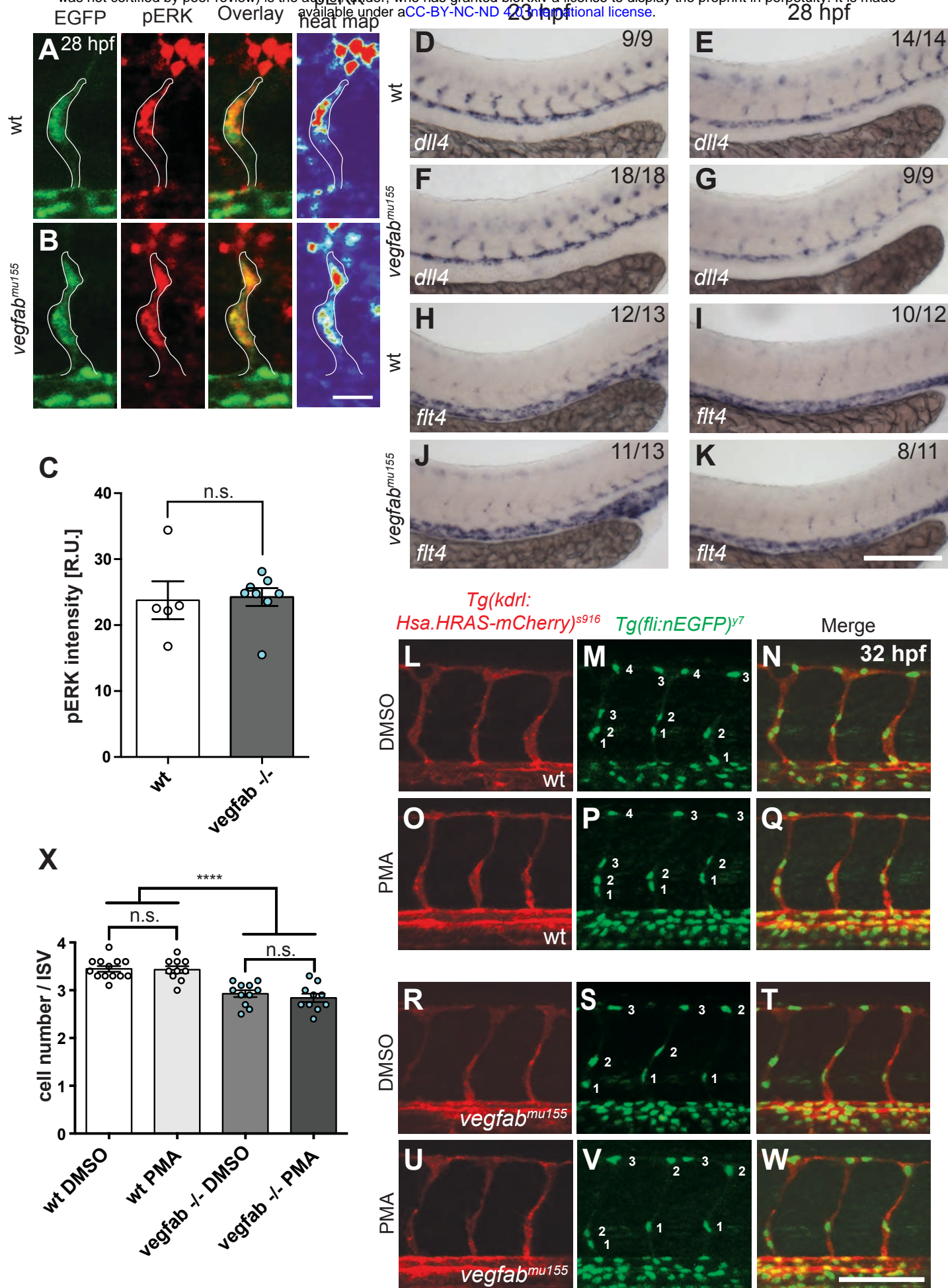
14   Endothelial cell membranes (red) are marked by virtue of mCherry expression, while

15   endothelial cell nuclei express EGFP (green) in *Tg(kdrl:Hsa.HRAS-mCherry)$_{s916}$*;

16   *Tg(fli1:nEGFP)$_{y7}$* zebrafish Side view of trunk region, anterior to the left. Imaging starts

17   at 22 hpf and is carried out for 6 hours. Individual endothelial cells are marked by

18   arrowheads and numbers. Decimal numbers indicate progeny after division.

19

20   **Supplementary Video S15. Endothelial cell proliferation and migration in**

21   **individual intersegmental blood vessel sprout in LY294002 treated zebrafish**
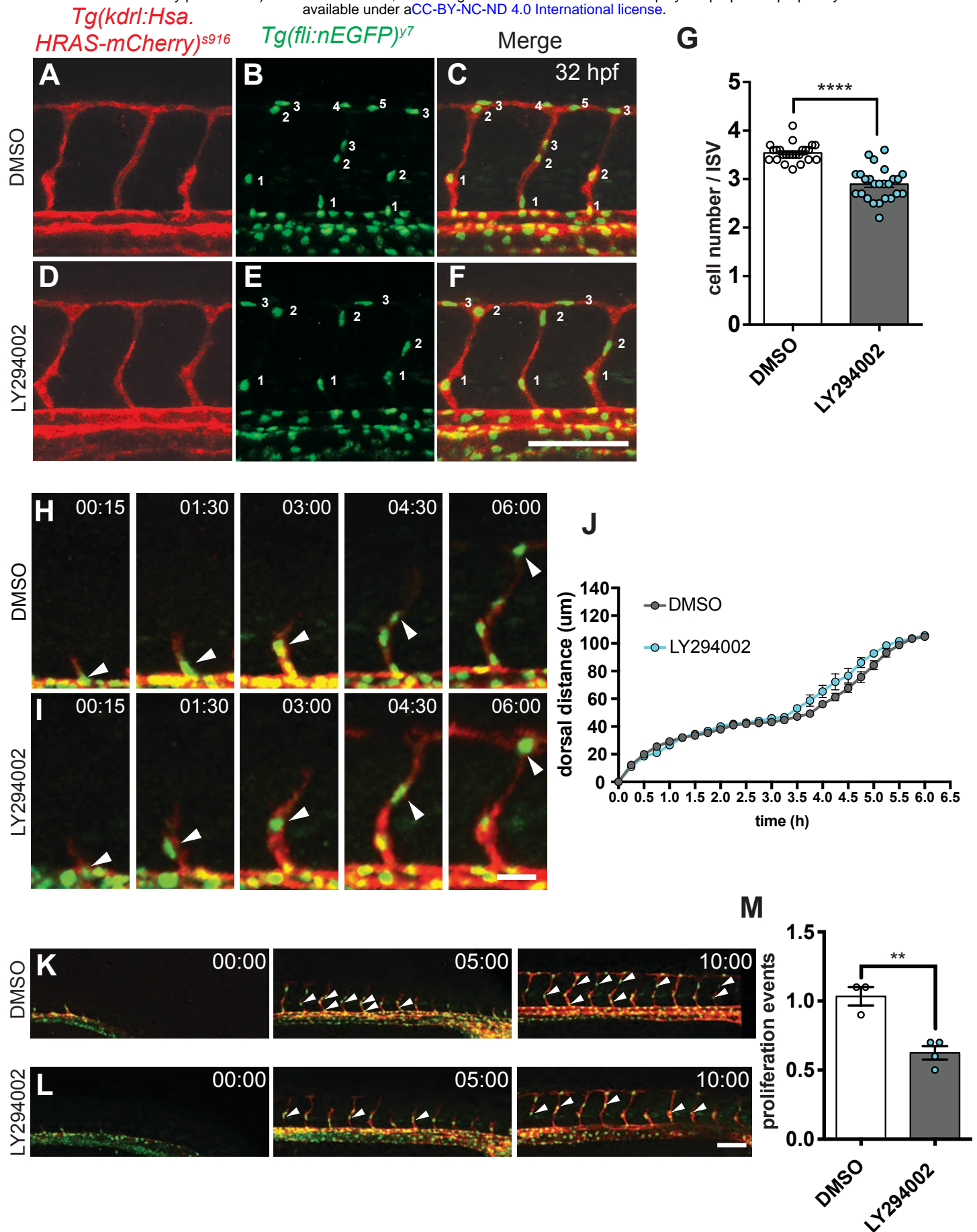
22   **embryo**

1   Endothelial cell membranes (red) are marked by virtue of mCherry expression, while

2   endothelial cell nuclei express EGFP (green) in *Tg(kdrl:Hsa.HRAS-mCherry)s916*;

3   *Tg(fli1:nEGFP)y7* zebrafish Side view of trunk region, anterior to the left. Imaging starts

4   at 22 hpf and is carried out for 6 hours. Individual endothelial cells are marked by

5   arrowheads and numbers. Decimal numbers indicate progeny after division.

6

7   **Supplementary Video S16. Endothelial cell proliferation and migration in**

8   **intersegmental blood vessel sprouts in DMSO treated zebrafish embryo**

9   Endothelial cell membranes (red) are marked by virtue of mCherry expression, while

10   endothelial cell nuclei express EGFP (green) in *Tg(kdrl:Hsa.HRAS-mCherry)s916*;

11   *Tg(fli1:nEGFP)y7* zebrafish. Side view of trunk region, anterior to the left. Imaging starts

12   at 22 hpf and is carried out for 10 hours. Individual endothelial cells are marked by

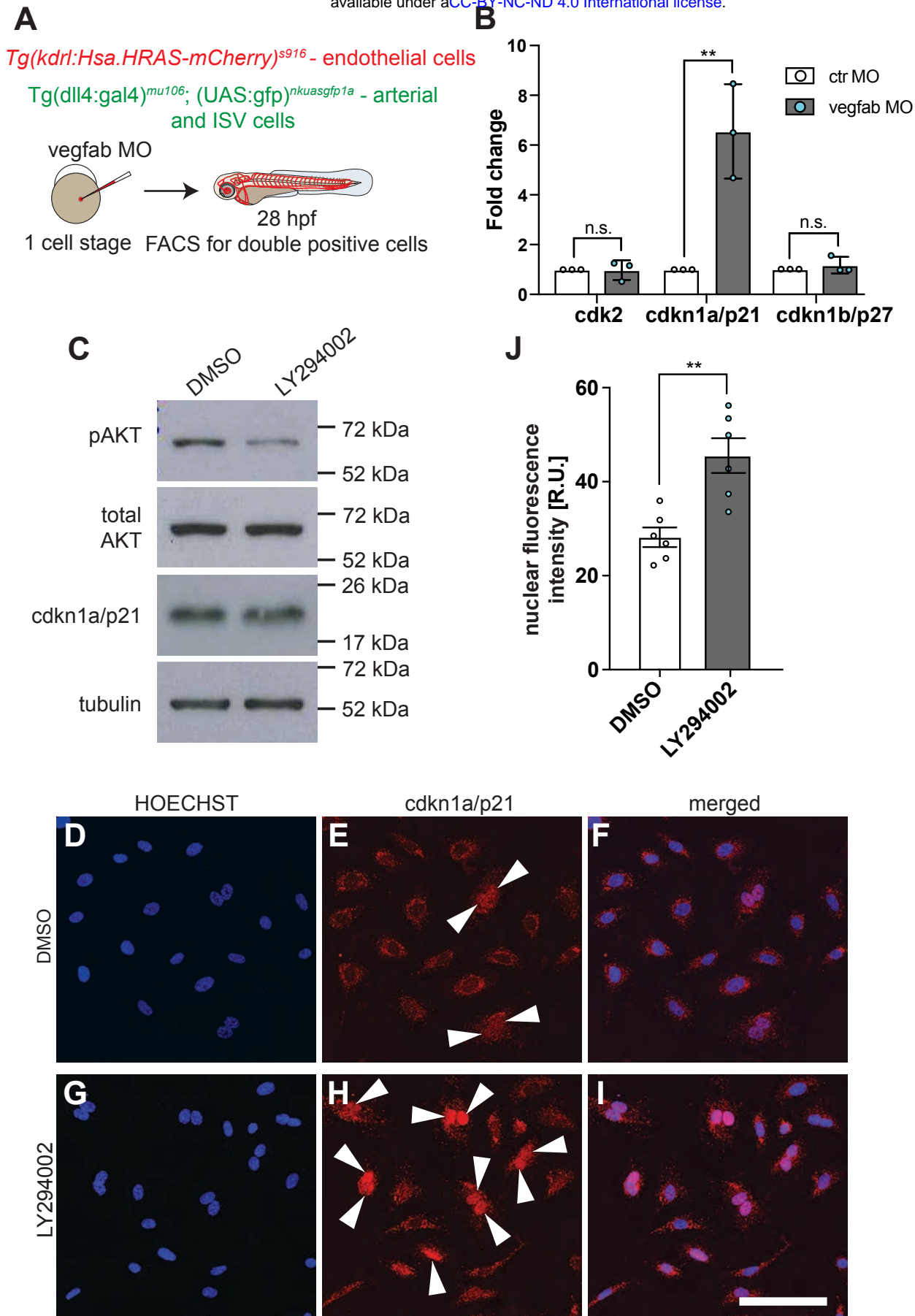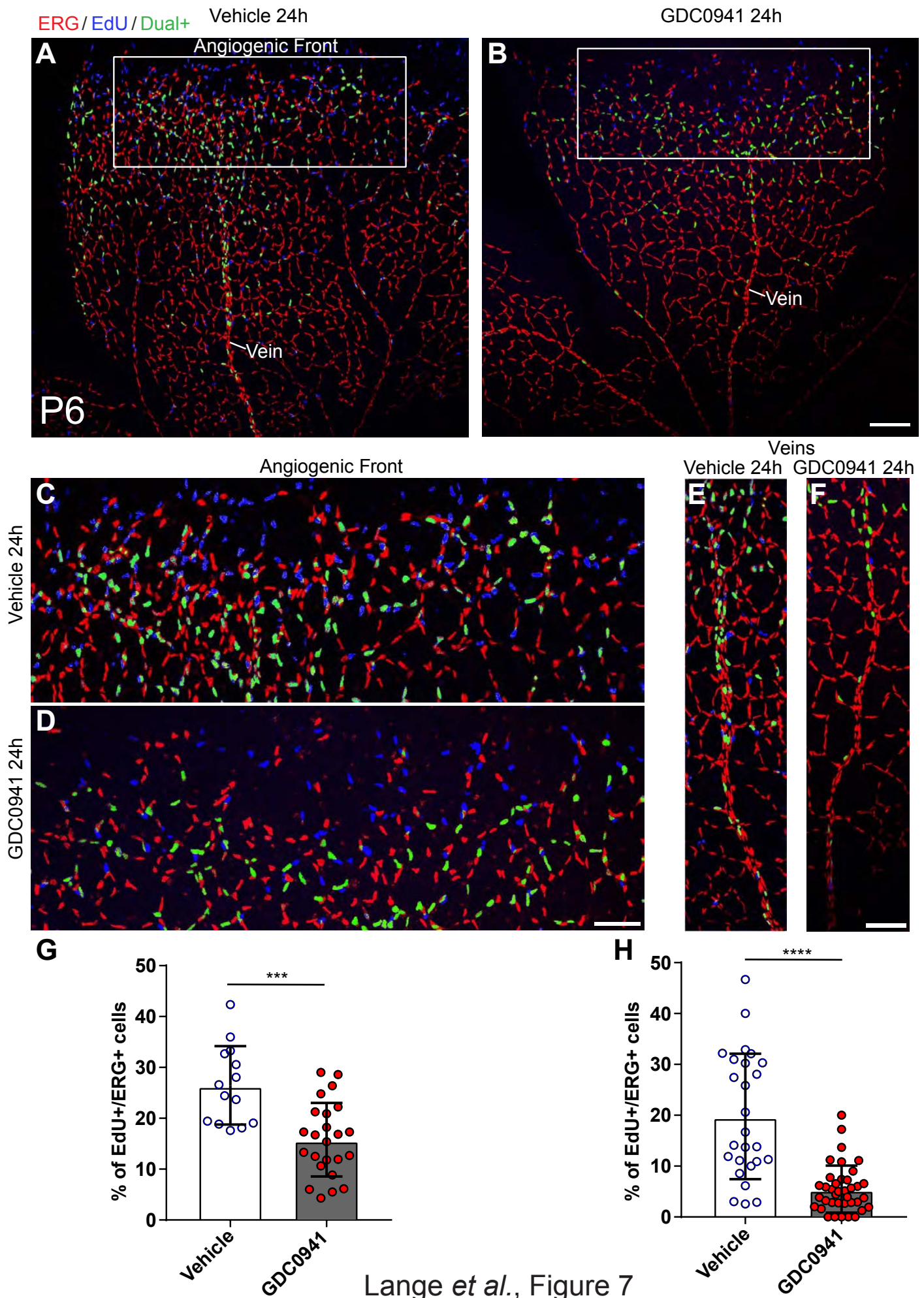13   arrowheads and numbers. Decimal numbers indicate progeny after division.

14

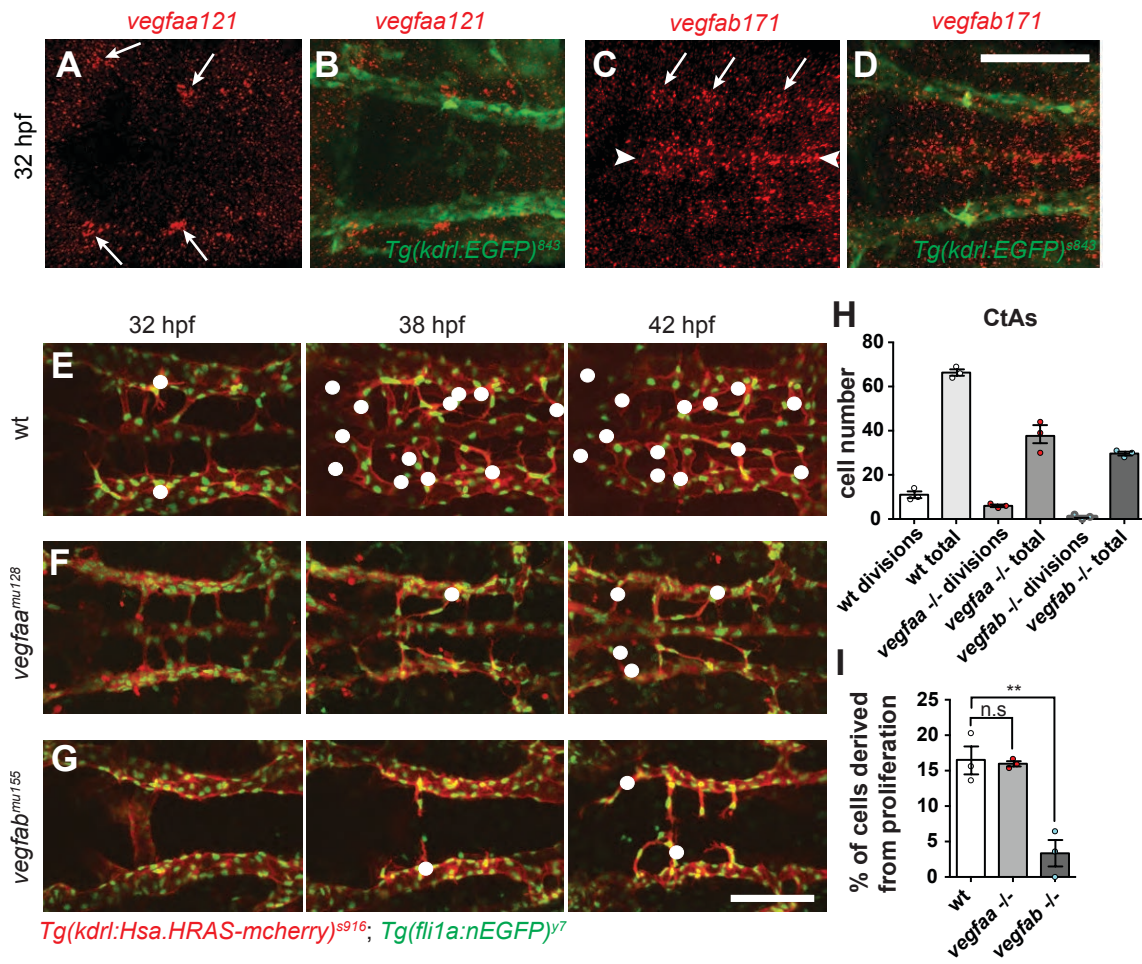15   **Supplementary Video S17. Endothelial cell proliferation and migration in**

16   **intersegmental blood vessel sprouts in LY294002 treated zebrafish embryo**

17   Endothelial cell membranes (red) are marked by virtue of mCherry expression, while

18   endothelial cell nuclei express EGFP (green) in *Tg(kdrl:Hsa.HRAS-mCherry)s916*;

19   *Tg(fli1:nEGFP)y7* zebrafish. Side view of trunk region, anterior to the left. Imaging starts

20   at 22 hpf and is carried out for 10 hours. Individual endothelial cells are marked by

21   arrowheads and numbers. Decimal numbers indicate progeny after division.

22

23

Lange *et al.*, Figure 1

Lange *et al.*, Figure 2

Lange *et al.*, Figure 3

Lange *et al.*, Figure 4

A

Tg(kdrl:Hsa.HRAS-mCherry)[s916] - endothelial cells

Tg(dll4:gal4)[mu106]; (UAS:gfp)[nkuasgfp1a] - arterial and ISV cells

vegfab MO

1 cell stage FACS for double positive cells

28 hpf

B

C

J

HOECHST   cdkn1a/p21   merged

D **E** **F**

DMSO

G **H** **I**

LY294002

Lange *et al.*, Figure 5

Tg(kdrl:Hsa.HRAS-mCherry)[s916]*;Tg(fli:nEGFP)*[y7]

Lange *et al.*, Figure 6

Lange *et al.*, Figure 7

Lange *et al.*, Supplementary Figure S1

Lange *et al.*, Supplementary Figure S2

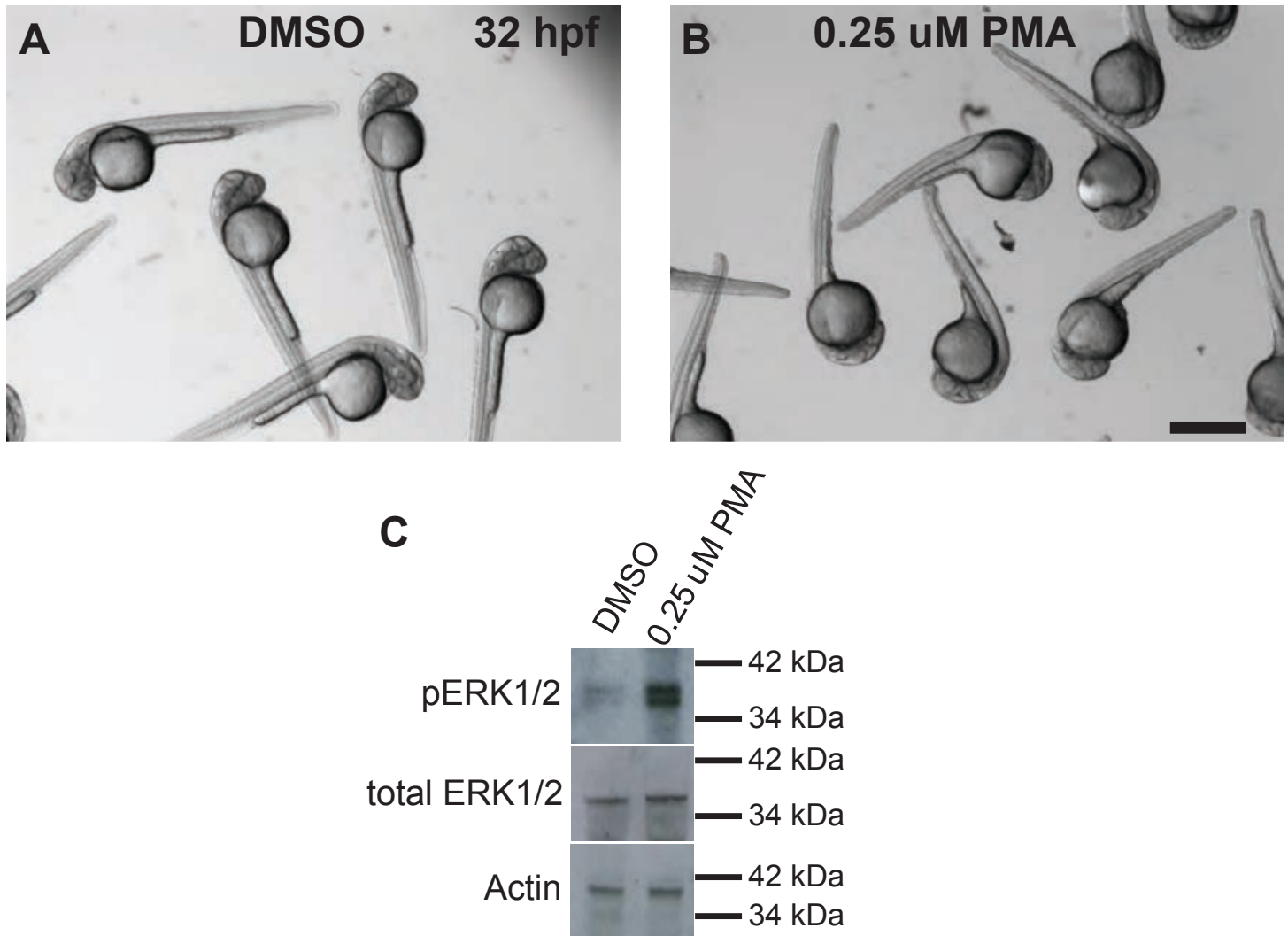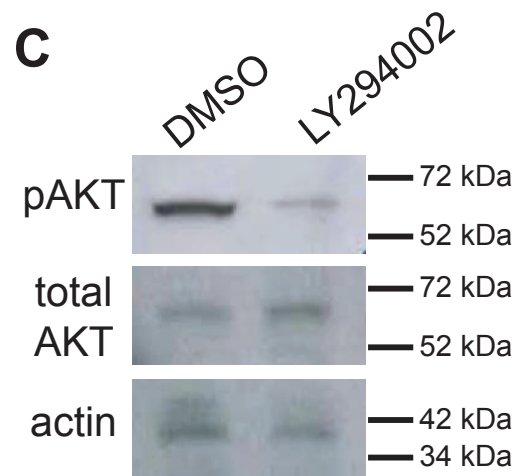*Tg(fli:nEGFP)^{y7};Tg(kdrl:Hsa.HRAS-mCherry)^{s916}*
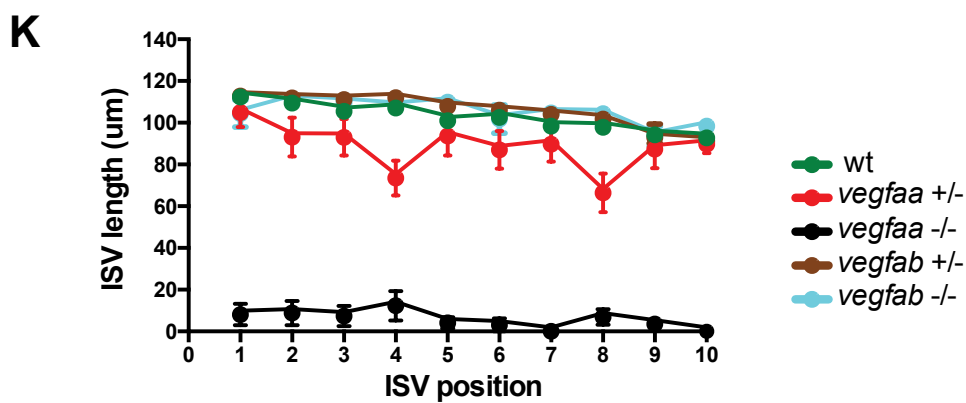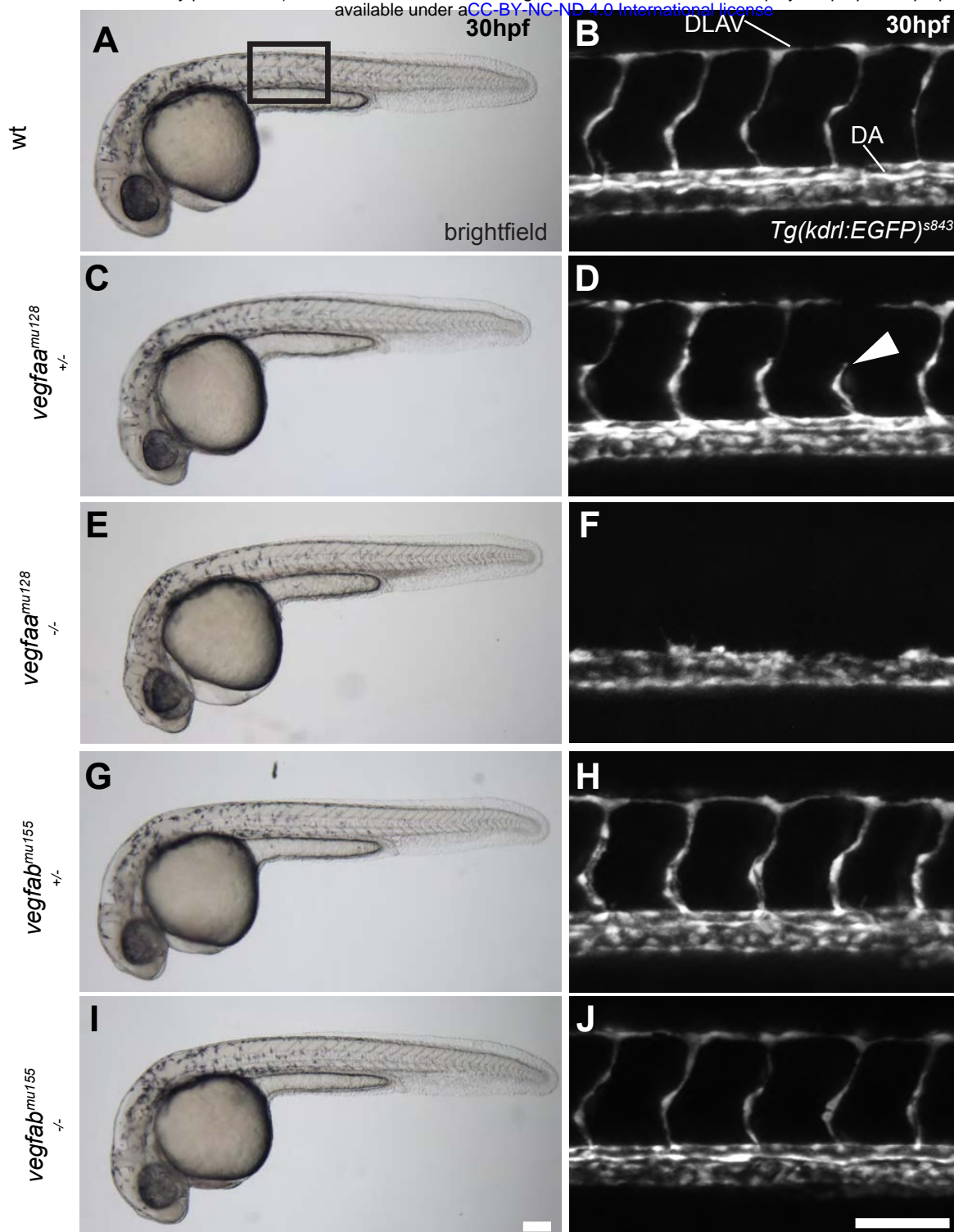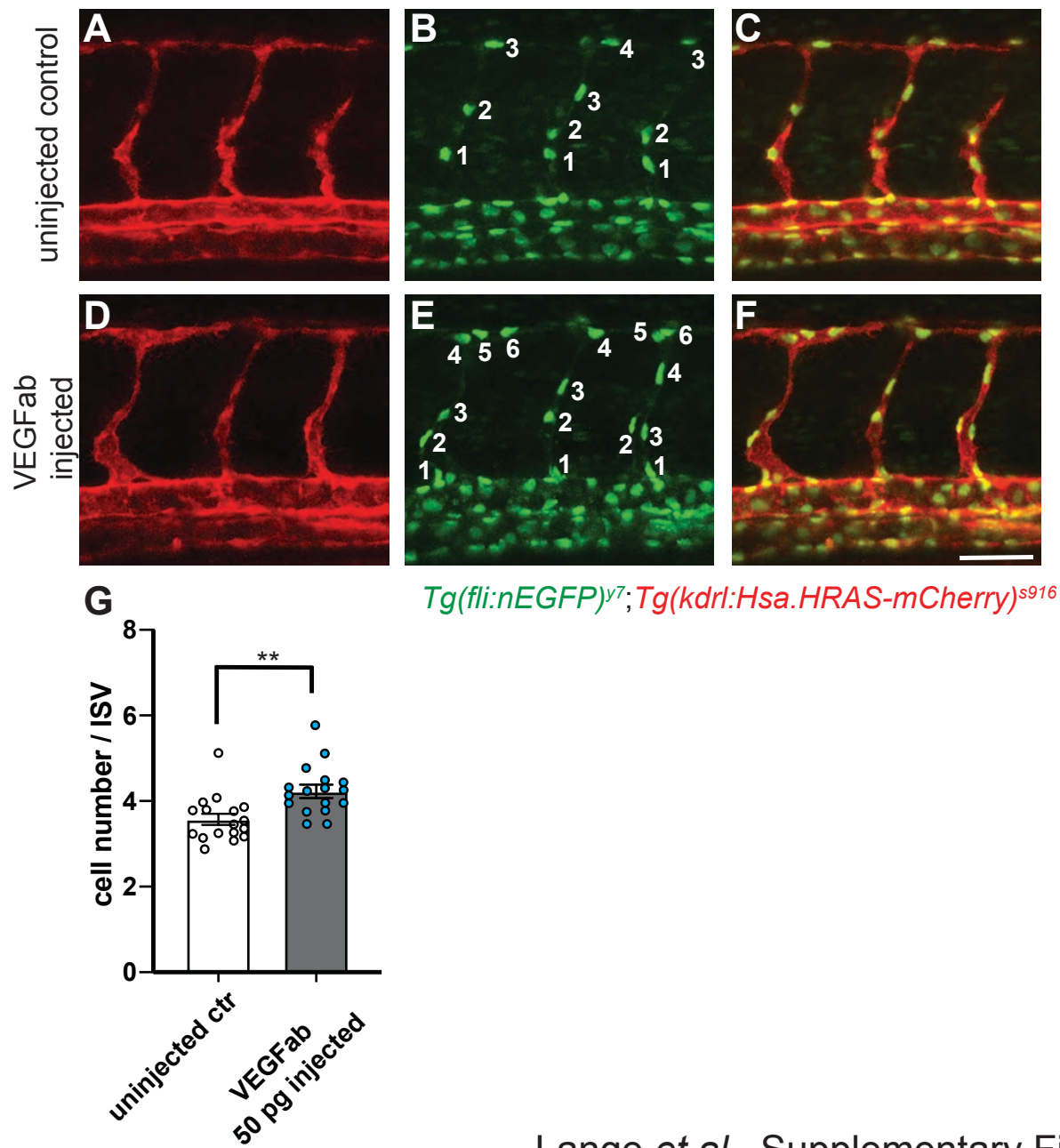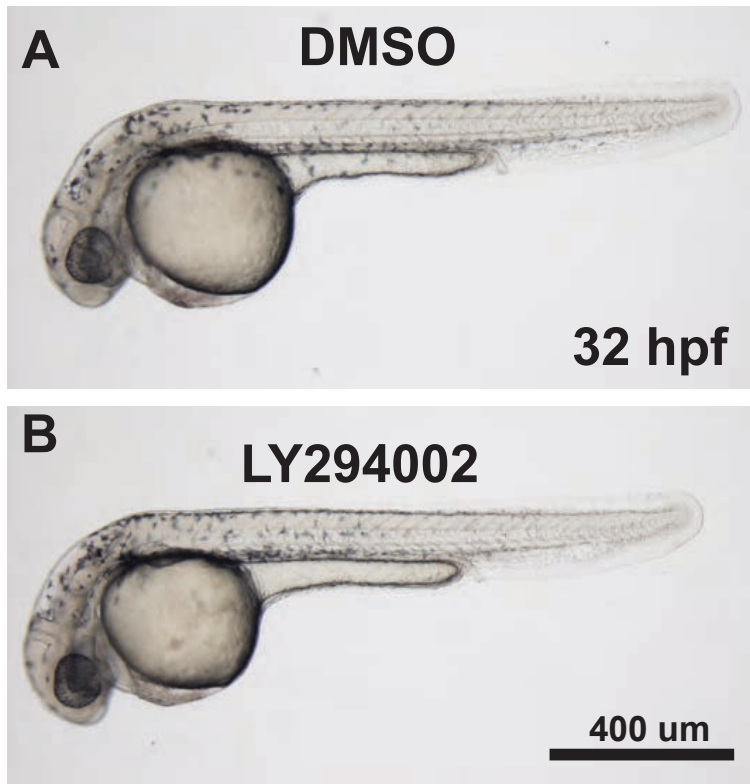
Lange *et al.*, Supplementary Figure S3

Lange *et al.*, Supplementary Figure S4

Lange *et al.*, Supplementary Figure S5

Lange et al., Supplementary Figure S6

Lange *et al.*, Supplementary Figure S7